Report SA-ALC/MMEP/88-02

INSPECTION DEVELOPMENT FOR T-37 WING SPAR CAP LUG

Jay L. Fisher
Gary L. Burkhardt
Stephen N. Rowland, Jr.
John H. Fitzgerald
Robert J. Dexter
Janet P. Buckingham

Southwest Research Institute
6220 Culebra Road
San Antonio, TX 78284

June 1989

Final Report for Period October 1, 1988, to June 30, 1989
Performed as a special task for the Nondestructive Testing Information Analysis Center under Contract DLA900-84-C-0910, CLIN 0001 BV

Prepared for
SAN ANTONIO AIR LOGISTICS CENTER/MMEP
Kelly Air Force Base, TX 78241

SOUTHWEST RESEARCH INSTITUTE
SAN ANTONIO HOUSTON

UNCLASSIFIED
SECURITY CLASSIFICATION OF THIS PAGE

REPORT DOCUMENTATION PAGE

Form Approved
OMB No 0704-0188

1a REPORT SECURITY CLASSIFICATION: Unclassified	1b RESTRICTIVE MARKINGS
2a SECURITY CLASSIFICATION AUTHORITY	3 DISTRIBUTION/AVAILABILITY OF REPORT: Approved for public release; distribution unlimited
2b DECLASSIFICATION/DOWNGRADING SCHEDULE	
4 PERFORMING ORGANIZATION REPORT NUMBER(S): 17-7958-851	5 MONITORING ORGANIZATION REPORT NUMBER(S)
6a NAME OF PERFORMING ORGANIZATION: Southwest Research Institute; 6b OFFICE SYMBOL (If applicable)	7a NAME OF MONITORING ORGANIZATION: San Antonio Air Logistics Center
6c ADDRESS (City, State, and ZIP Code): P.O. Drawer 28510, San Antonio, Tx 78284	7b ADDRESS (City, State, and ZIP Code): ATTN: MMEP, Kelly AFB, TX 78241
8a NAME OF FUNDING/SPONSORING ORGANIZATION: Defense Logistics Agency; 8b OFFICE SYMBOL (If applicable): DTIC-DF	9 PROCUREMENT INSTRUMENT IDENTIFICATION NUMBER: DLA900-84-C-0910, CLIN 0001BV
8c ADDRESS (City, State, and ZIP Code): DTIC, Cameron Station, Alexandria, VA 22304	10 SOURCE OF FUNDING NUMBERS: PROGRAM ELEMENT NO; PROJECT NO; TASK NO; WORK UNIT ACCESSION NO

11 TITLE (Include Security Classification): Inspection Development for T-37 Wing Spar Cap Lug

12 PERSONAL AUTHOR(S): Fisher, Jay L.; Burkhardt, Gary L.

13a TYPE OF REPORT	13b TIME COVERED	14 DATE OF REPORT (Year, Month, Day)	15 PAGE COUNT
Final	FROM 10/1/88 TO 6/30/89	1989 June 30	

16 SUPPLEMENTARY NOTATION: Performed as a Special Task for the Nondestructive Testing Information Analysis Center

17 COSATI CODES			18 SUBJECT TERMS (Continue on reverse if necessary and identify by block number)
FIELD	GROUP	SUB-GROUP	

19 ABSTRACT (Continue on reverse if necessary and identify by block number)

The purpose of this project was to develop an eddy current nondestructive inspection technique and procedure for the fatigue-critical location on the lower cap lug fillet of the T-37 wing spar, and to develop and conduct an inspection reliability program to quantify the inspection capability. The inspection capability goal was to demonstrate a probability of detection of 90 percent with a 95 percent confidence level for 0.050-inch radius fatigue cracks in the critical region of the lug. A hand-operated mechanical probe manipulator was developed to ensure uniform inspection results. A set of test specimens with fatigue cracks was fabricated for the reliability study. All of the goals were met or exceeded in the program.

20 DISTRIBUTION/AVAILABILITY OF ABSTRACT	21 ABSTRACT SECURITY CLASSIFICATION
☒ UNCLASSIFIED/UNLIMITED ☐ SAME AS RPT ☐ DTIC USERS	Unclassified
22a NAME OF RESPONSIBLE INDIVIDUAL: Paul Schattle	22b TELEPHONE (Include Area Code): (512) 925-6408; 22c OFFICE SYMBOL: SA-ALC/MMEP

DD Form 1473, JUN 86 — Previous editions are obsolete — SECURITY CLASSIFICATION OF THIS PAGE

TABLE OF CONTENTS

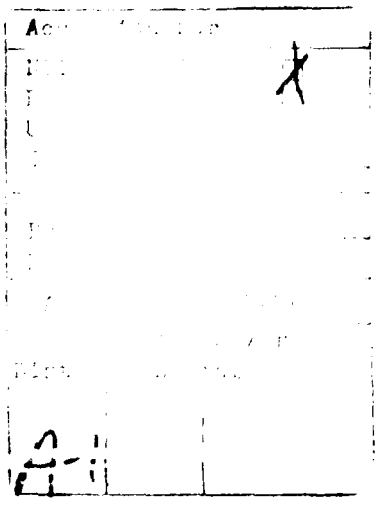

LIST OF FIGURES

LIST OF TABLES

1. INTRODUCTION AND SUMMARY

A damage tolerance analysis (DTA) conducted by Cessna Aircraft Company for the Air Force revealed fatigue-critical locations on the T-37 aircraft. From this analysis, the Air Force determined that the fatigue-critical region of the wing front spar lower cap lug (Figure 1-1) is the driver for determining minimum inspection intervals for this aircraft. In order to avoid multiple inspections of the T-37 fleet before the Service Life Extension Program (SLEP) provides modifications to this part, an improved defect detection capability was desired.

The purpose of this project was to develop a nondestructive inspection (NDI) technique and procedure for the fatigue-critical location on the lower cap lug fillet, and to develop and conduct an inspection reliability program to quantify the inspection capability. The inspection capability goal was to demonstrate a probability of detection (POD) of 90 percent with a 95 percent confidence level for 0.050-inch radius fatigue cracks in the critical region of the lug. All of these goals were met or exceeded in the program.

It was determined that the most appropriate examination for field use was eddy current testing (ET). In order to provide a uniform surface for ET, the Air Force arranged in a separate project to develop a machining device to produce a uniform bevel in the critical region, to replace the hand-worked radius in production aircraft. The uniform geometry also allowed development of a hand-operated mechanical probe manipulator to ensure uniform inspection results. A simplified drawing of the modified geometry and the critical cracks and their locations is shown in Figure 1-2. Two critical crack types were defined, as shown in the figure: a surface crack, in which the flaw surface lies entirely within the bevel face; and a corner crack, in which half of the flaw surface is on the bevel and half is on the vertical side of the lug. This geometry was used for development of the NDI technique and for specimens manufactured by SwRI for the reliability study.

After development of the inspection device and procedure, personnel from Lear Siegler, Inc. (LSI) and the Air Force were trained in the inspection procedure. At that time, aircraft inspections were started at Randolph AFB and McClellan AFB.

For determining POD, test specimens with fatigue cracks were produced. Four inspectors (two from LSI, one from McClellan AFB, and one from SwRI) inspected the fatigue crack specimens at SwRI to provide a POD database. These tests showed that the initial goal of 90 percent POD of 0.050-inch cracks with a 95 percent confidence level was surpassed, and that smaller flaws were consistently detected.

The remainder of this report presents a discussion of the ET technique development (Section 2), test specimen preparation (Section 3), and inspection reliability test analysis (Section 4). The results are summarized in Section 5. The Appendix contains the procedure developed for field inspections; it also describes the inspection device and shows typical results of the inspection on EDM notches and fatigue cracks.

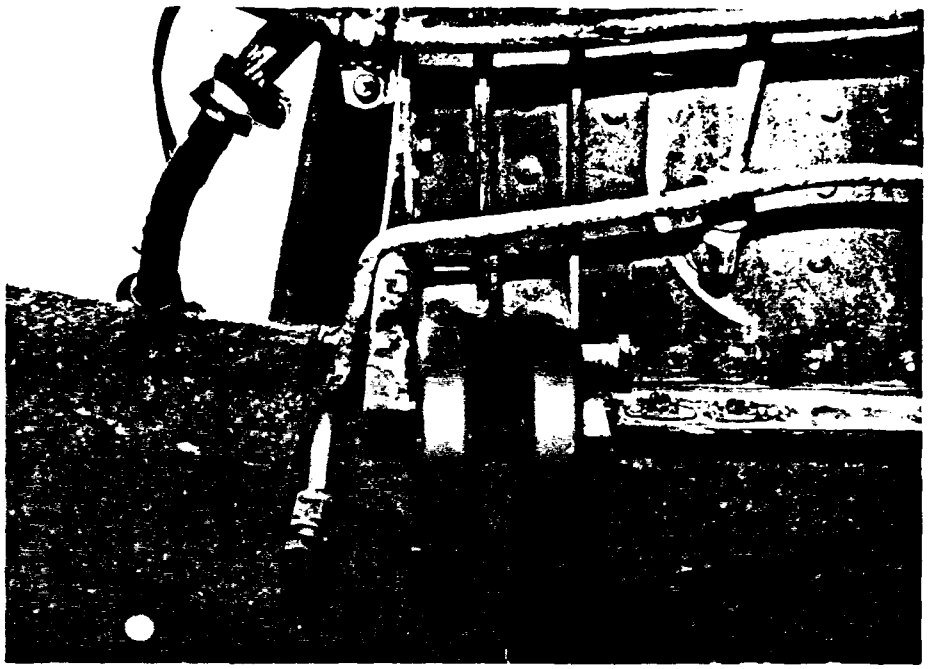

Figure 1-1. Typical lower cap lug of a T-37 wing front spar, shown before modifications to enable reliable examination.

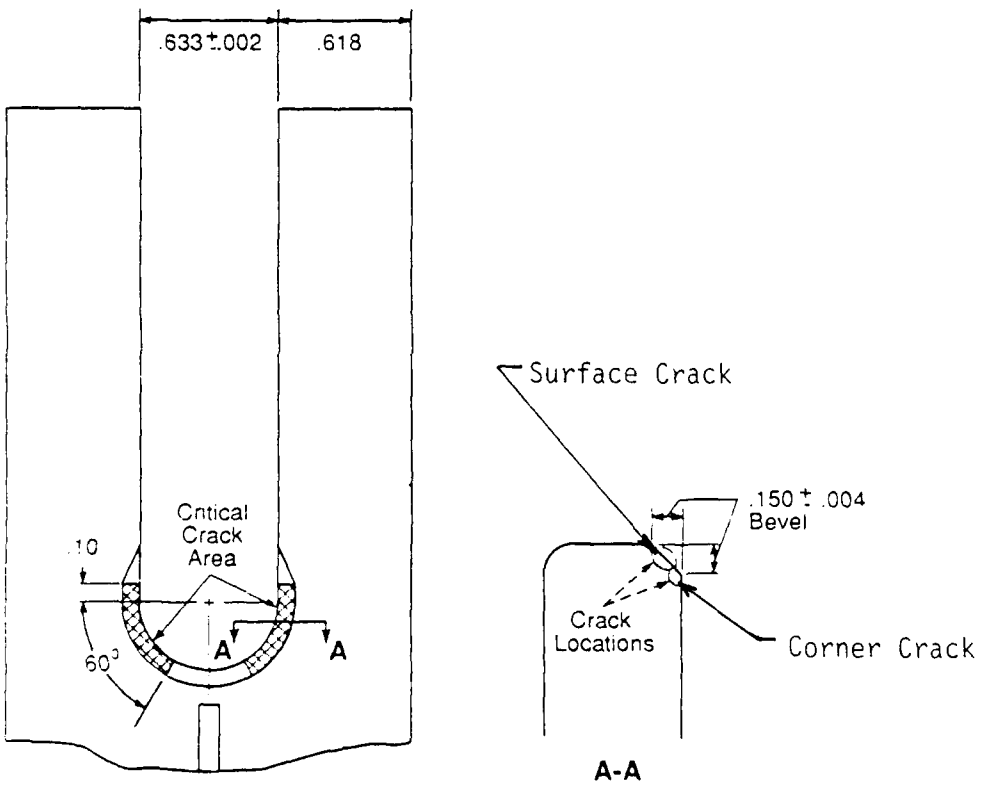

Figure 1-2. Drawing of the modified geometry of the lug, showing the critical inspection area and critical flaw locations.

2. TECHNIQUE DEVELOPMENT

Three types of eddy current probes were tested for this application: absolute, unshielded differential, and shielded differential coils. The probes were tested on a specimen with EDM notches of 0.030-, 0.040-, and 0.050-inch radii on the bevel surface and at the bevel-radius edge at the locations shown in Figure 1-2. Initial tests were conducted by mounting the eddy current coil in a holder for manual scanning.

An impedance plane display eddy current instrument (Stavely Instruments NDT-19) was procured for technique development. It was chosen because (1) previous tests by SwRI had shown that this instrument has sensitivity equal to or better than several other competing instruments, (2) it has two-frequency capability, and (3) it has a composite video output that can be used as input to a VCR for documenting inspections.

Initial tests revealed that all EDM notches could be detected with all of the probe types evaluated, but that edge effects resulting from scans near the bevel edge could be minimized by using the shielded differential probe. These tests also showed that the optimum frequency range for operation with this probe was 300-400 kHz. Therefore, this frequency range and probe type were chosen for further development.

It was also determined early in the project that a manual, unmechanized procedure would not provide the desired flaw detection reliability. Therefore, it was decided to develop an inspection device that would include a manually operated probe manipulator to ensure that the probe would follow the bevel approximately parallel to the bevel edges. This probe manipulator assembly is shown in Figures 3 and 4 in the Appendix.

The manipulator body is inserted between the arms of the lug and is secured in place by keying on the bolt holes in the lugs. The probe is spring-loaded at a constant angle with respect to the inspection surface to provide a uniform background signal. In order to follow the bevel surface, the probe is rotated about the axis of the probe manipulator, and a cam sleeve on the manipulator provides vertical motion to follow the vertical contour of the lug. The radial position of the probe is adjustable to provide a series of scans at different heights along the bevel surface. The probe tip is coated with aluminum oxide to provide a permanent wear surface, avoiding the need for tape to protect the coils.

An inspection is conducted by first mounting the probe manipulator on the calibration specimen, performing calibration, then mounting the probe manipulator on the aircraft wing and performing the inspection and recording the results. This inspection procedure is detailed in the Appendix.

After development of the inspection device and the procedure, personnel from LSI (Randolph AFB) and the Air Force (McClellan AFB) were trained in the inspection procedure. One inspection kit was delivered to the Air Force, and, under a separate contract, two other identical kits were delivered to LSI.

During initial inspections after the training, three problems occurred in the field. One was that the probe manipulator body would not fit between the fingers of the lug on some aircraft; it was determined that the lugs had been bent and were out of tolerance of the aircraft drawings. The solution was to machine the sides of the probe manipulator body to allow insertion. A second problem was the presence of a response to probe motion when the direction of rotation of the probe manipulator was reversed. This response made it difficult for inspectors to accurately determine the liftoff response of the probe. The solution was to reduce the tension of the spring holding the probe against the surface. A third problem was that the direction of probe liftoff variation response in the impedance plane was not consistent among the different probes. This condition was caused by the fact that liftoff response is not consistent among differential probes, because the liftoff response is an artifact of the imprecise matching of the two coils in the probe. The procedure had to be modified to allow use of all probes manufactured for the inspection. After these changes were made, the inspections continued without known problems.

3. TEST SPECIMEN PREPARATION

3.1 Introduction

The purpose of this task was to produce fatigue cracks in test specimens that simulate the reworked fatigue-critical area in the T-37 wing front spar lower cap lug. These specimens were used in the reliability tests to determine the POD. The specimens were fabricated from 7075-T73511 aluminum extruded bar, the same type of material as used in the wing spar. The specimens were subjected to cyclic loading to produce either surface cracks on the lug bevel surface, or corner cracks located at the intersection of the bevel with the lug radius (the curved part of the vertical surface of the lug), as shown in Figure 1-2. Dummy specimens without cracks were also fabricated. Table 3-1 lists the crack sizes and numbers of specimens required and produced.

3.2 Specimen Geometry

Each specimen has two surfaces, each of which represents half of the aircraft wing spar lug. Thus, two specimens are mated to form two inspection surfaces for the reliability tests. This geometry was chosen to reduce machining costs and to provide a means for precracking two halves simultaneously. Also, in order to minimize manufacturing costs, the specimens were manufactured with flat horizontal surfaces (where the orientation referred to is that of the lug in the aircraft) on the top and bottom. This geometry differs only slightly from that of the critical area of the aircraft lug, in which the spar upper surface rises to form the lug, as can be seen in Figure 1-1. This geometry also allowed the bevel to be formed as a countersink in the lug surface. The geometry at different construction stages will be discussed in following sections.

3.3 Basic Fabrication Procedure

The basic test procedure included the following:

(1) Precracking was performed with a 10-kip maximum capacity MTS, closed-loop, electro-hydraulic testing system. The specimens were fatigued in bending under constant amplitude cyclic loading at a stress ratio (R) of 0.1. One end of the specimen was attached to a very stiff fixture and the other was cantilevered and loaded near the end. The maximum stress yielded an initial crack tip stress intensity (K) of approximately

10 ksi$\sqrt{in}$. The overall test setup and the use of an inspection mirror for monitoring the crack growth are shown in Figure 3-1.

(2) Crack starter flaws were introduced at the desired locations by electron discharge machining (EDM). The EDM cutting tool was prepared to produce a thin triangular (90° angle) shaped flaw 0.02 inch deep with a surface length of 0.04 inch.

Table 3-1

TEST MATRIX FOR T-37 LUG SPECIMENS

Nominal Crack Size (a)* (inch)	Number Required	Number Produced
	Surface-Cracked Specimens	
0.03	6	6
0.04	7	7
0.05	15	20
0.06	2	5
	Corner-Cracked Specimens	
0.03	6	8
0.04	7	9
0.05	15	15
0.06	2	5
	Dummy Specimens (No Flaws)	
NA	20	20

*The nominal crack size (a) is 1/2 the total surface length.

(3) The surface crack specimens (Configuration 1) were machined as shown in Figure 3-2 and included a subdepth (0.11 inch) countersink. After precracking, the countersink depth was increased to the required dimension (0.15 inch). This operation removed the EDM preflaw but retained a portion of the precrack (see Figure 3-3a).

(4) The corner crack specimens (Configuration 2) were machined as shown in Figure 3-4 and included a subsize radius (0.277 inch) and full depth countersink. Following precracking, the specimens were machined to the required radius (0.317 inch) and then recountersunk to the final depth. This procedure is illustrated in Figure 3-5b.

3.4 Experiments to Determine Crack Shapes and Final Sizes

It is evident from Figure 3-3 that an *a priori* knowledge of the crack growth behavior would be necessary in order to accurately predict the final crack shapes and sizes remaining after the final machining operations. Therefore, an experimental task was initiated and included the testing of four specimens from each configuration (Figures 3-2 and 3-4).

The first two surface-flawed specimens, I.D. numbers 1A and 1B, were prepared with EDM crack starter slots at or near the center of the countersunk surface. Following precracking, the specimens were weakened by saw cuts and broken to reveal the fractured surfaces. Photographs of the resulting crack shapes are shown in Figure 3-5. In both cases, the cracks grew more rapidly in the direction of the radius, that is, toward the location having the highest stress. Fatigue "range marks" were introduced on the fracture surface of specimen number 1B by periodically increasing the stress ratio. This effort highlighted the accelerated growth of the crack as it entered the radiused section, shown in Figure 3-5b. The grossly oversized crack produced in this experiment provided insight into a technique that was particularly useful for the estimation of crack sizes in corner-flawed specimens. This technique will be discussed later.

The first two corner-flawed specimens, I.D. numbers 2A and 2B, were prepared with EDM slots. The centerline of the slot was located approximately 0.05 inch (specimen 2A) and 0.03 inch (specimen 2B) from the intersection of the radius and countersink. Pictures of the post-precrack fractures from these experiments are shown in Figure 3-6.

The remaining four specimens, two of each configuration, were also prepared with EDM slots. The slot location for corner flaws was similar to the previous experiments; however, for the surface flaws, the slot was located more toward the unradiused (free) edge of the countersink. This was done in order to compensate for the faster growth rates witnessed in the direction of the radius. The specimens were precracked to produce a short and long crack for each configuration. Note: The shortest anticipated crack half-length (a) at this stage of the program was 0.05-inch. Following precracking, the specimens were machined to the required final dimensions and were inspected with ET. The cracks were easily detected; therefore, the final test matrix (Table 3-1) included crack half-lengths of 0.03 and 0.04 inch.

The experimental test results provided a means for estimating crack sizes following the final machining operations. The technique treats the side of the countersink as though it were the diameter of a circle. For cracks within the countersink (surface flaws), the center of the circle is

simply half the distance between the measured ends of the crack. A compass is used to draw a semicircle, representing the precracked fracture, and the final crack length is determined. The procedure is illustrated for short and long cracks in Figure 3-7. Note that both the aspect ratio (crack depth/length) and accuracy of the prediction would tend to decrease with decreasing crack size.

As shown in Figure 3-8, a slightly more complicated procedure is used for cracks that enter the radius (corner cracks). The center of the circle is determined by adjusting a compass so that the perimeter of the semicircle passes through both visual measurements. It is interesting to note that the crack grows in a semicircular fashion even though there is no material between the initial radius and extension of the countersink.

Although the anticipated crack shape is circular, this method of crack fabrication produces cracks with depths less than half of the surface length, as shown in Figures 3-7 and 3-8. This result is caused by the fact that for both flaw types, the center of the semicircle lies outside of the final surface. In order to provide a conservative estimate for the reliability study, the crack size was considered to be one half of the estimated crack length rather than the estimated crack radius.

3.5 Specimen Preparation for Eddy Current Inspection

A careful study of the eight experimental test results provided a guide (see Table 3-2) for the optimum EDM slot location and precrack lengths that would produce the final crack sizes listed in Table 3-1. Each specimen contained one crack; however, for a given crack size, the cracks were equally distributed on the right- and left-hand sides of the specimens. Precracking and other pertinent information for each specimen was recorded on diagrams identical to those in Figures 3-7 and 3-8. The precracked specimens were machined to remove the EDM slot and were then fatigue loaded (approximately 50 cycles) to reopen the cracks because the machining operations tend to lap metal over the cracks. The specimens were then machined to the final configuration shown in Figure 3-9. This design included holes for pinning two selected specimens together to form one clevis. The locations of the transducer mounting holes simulate the actual T-37 clevis and allow for the inspection on either side of the test specimen.

The total number of specimens produced (including the uncracked dummy coupons) was 95; therefore, using this number as a seed, a random number (1 through 95) was generated to represent each specimen. This I.D. number was stamped on the thickest end of each specimen; the viewing orientation for determining the right- and left-hand side is illustrated in Figure 3-10.

Tables were prepared listing the I.D. number, basic code, nominal crack size code, and the estimated crack length. The code system included the following:

Basic Code	Meaning	Crack Size Code	Nominal Size (inch)
S	Surface Crack	1	0.03
C	Corner Crack	2	0.04
L	Crack on Left	3	0.05
R	Crack on Right	4	0.06

Example: An SR2 code would indicate a 0.04-inch surface crack located on the right-hand side of the specimen.

The tables were treated as "secret" and were provided to the inspection monitor only.

Table 3-2

EDM LOCATIONS AND PRECRACK LENGTHS

Surface-Cracked Specimens

Nominal Crack Size (a)* (inch)	EDM Centerline Distance from Free Edge (inch)	Total Precrack Length (inch)	Estimated Depth (inch)
0.03	0.070	0.080	0.013
0.04	0.065	0.100	0.021
0.05	0.060	0.118	0.029
0.06	0.050	0.130	0.038

Corner-Cracked Specimens

Nominal Crack Size (a)* (inch)	EDM Centerline Distance from Free Edge (inch)	Precrack Length (inch)		Estimated Depth (inch)
		Radius	Countersink	
0.030	0.025	0.038	0.068	0.016
0.040	0.025	0.045	0.075	0.024
0.050	0.035	0.055	0.085	0.031
0.060	0.035	0.065	0.095	0.038

*The nominal crack size (a) is 1/2 the total surface length (see Figures 3-7 and 3-8).

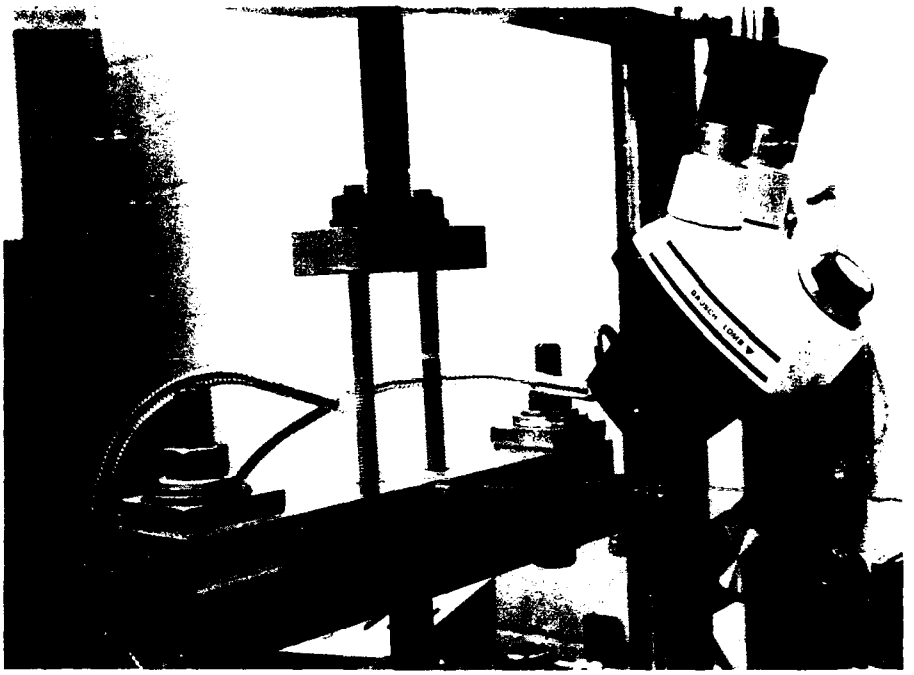

(a) Overall test setup

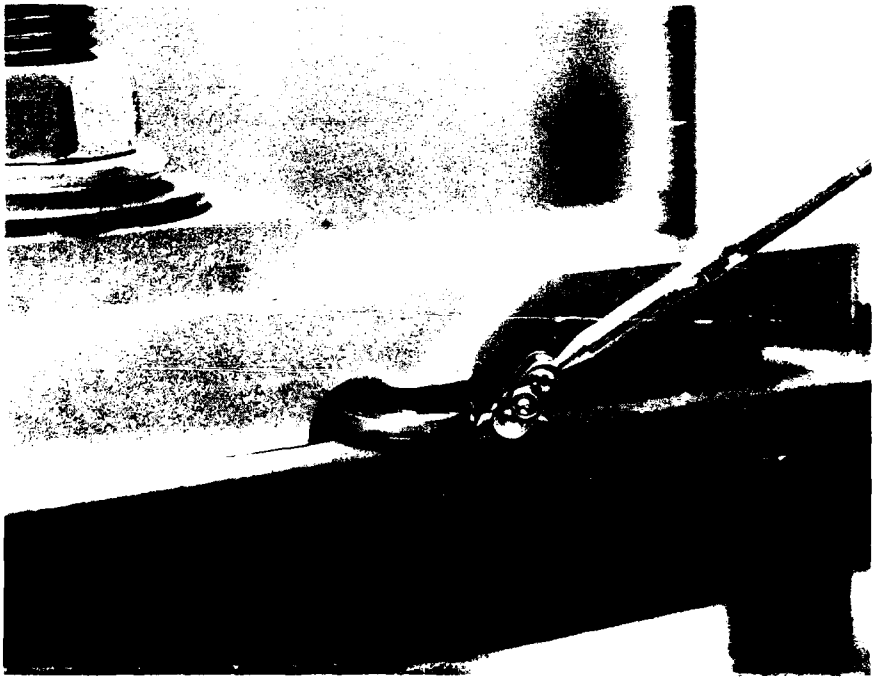

(b) Viewing a crack with inspection mirror

Figure 3-1. Test setup for precracking specimens

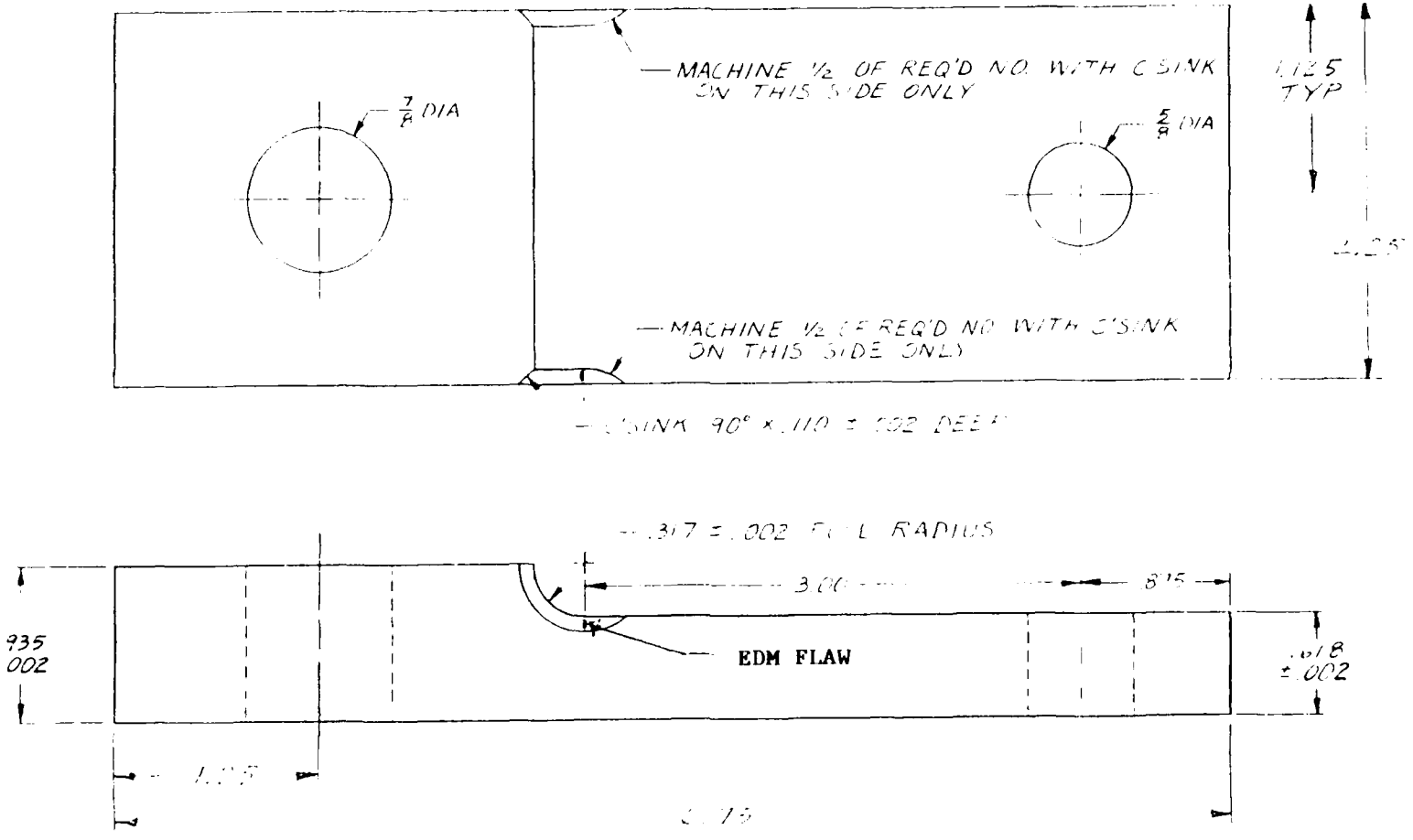

Figure 3-2. Initial configuration for surface cracked specimens

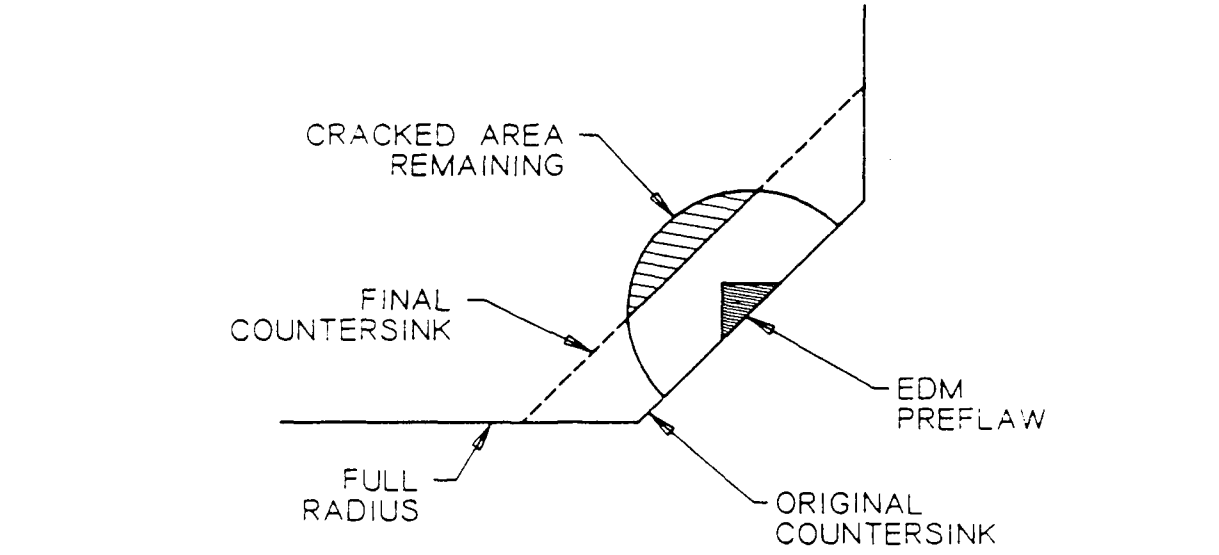

a) SURFACE CRACK

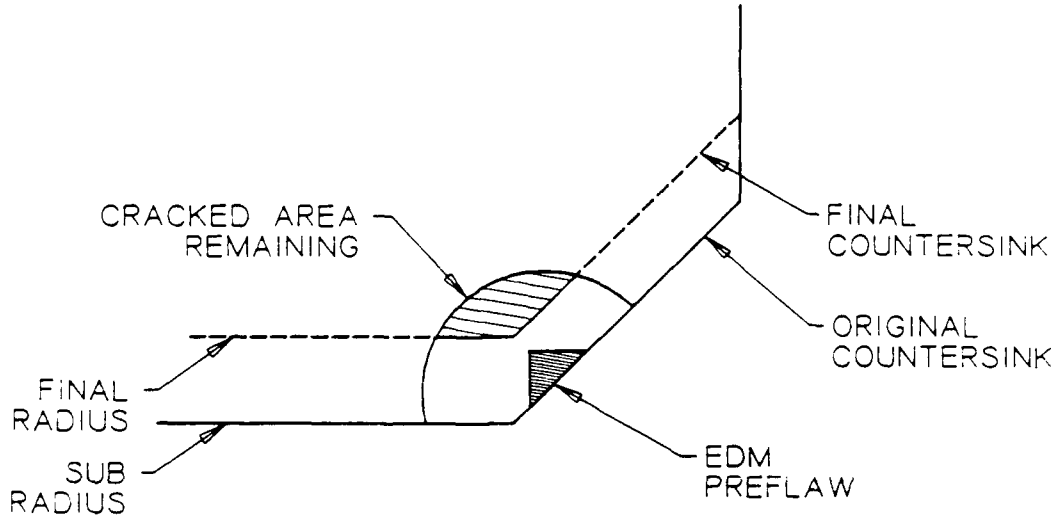

b) CORNER CRACK

Figure 3-3. Illustrations showing methodology for obtaining surface and corner cracks in test specimens

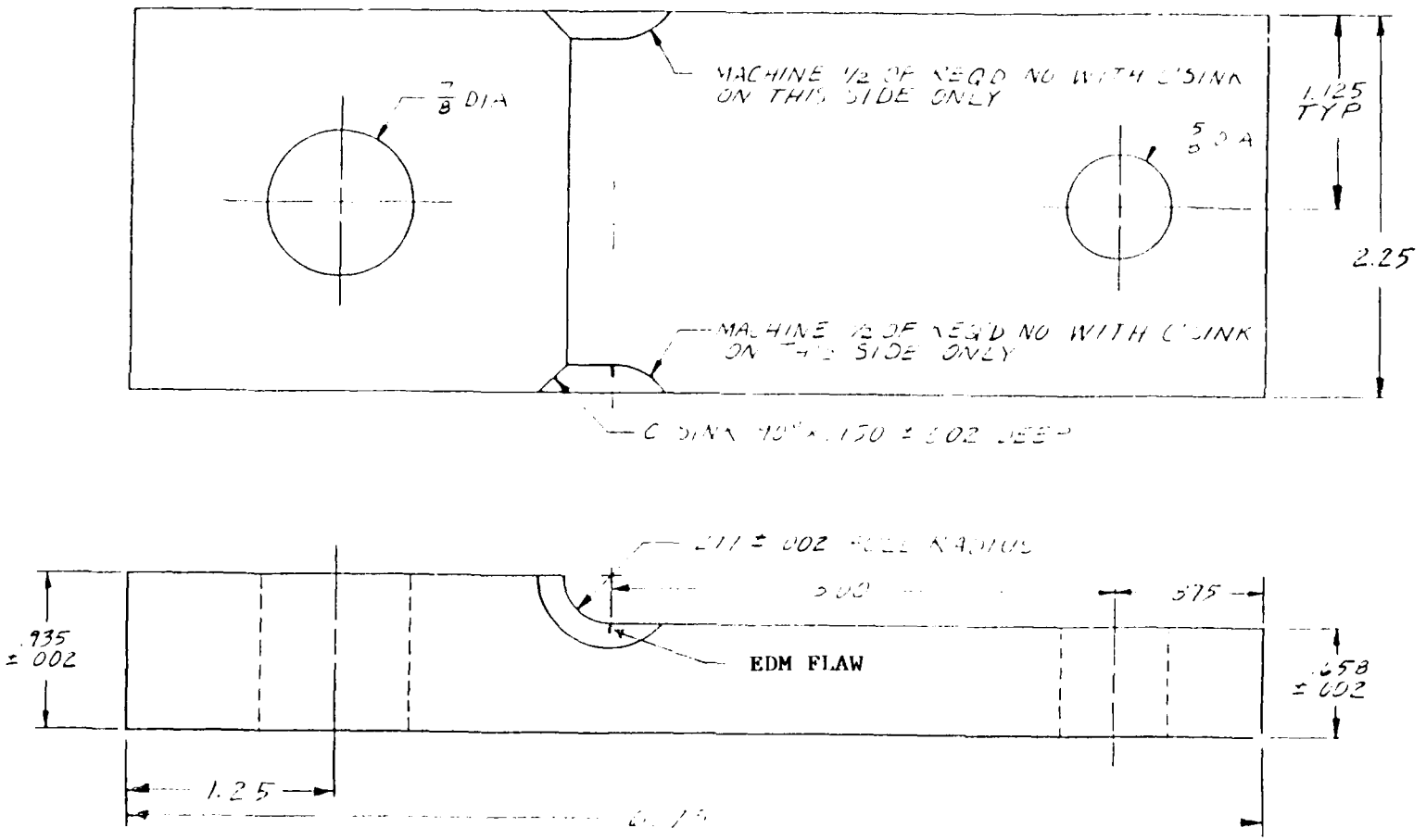

Figure 3-4. Initial configuration for

← Radius →

(a) Specimen number 1A

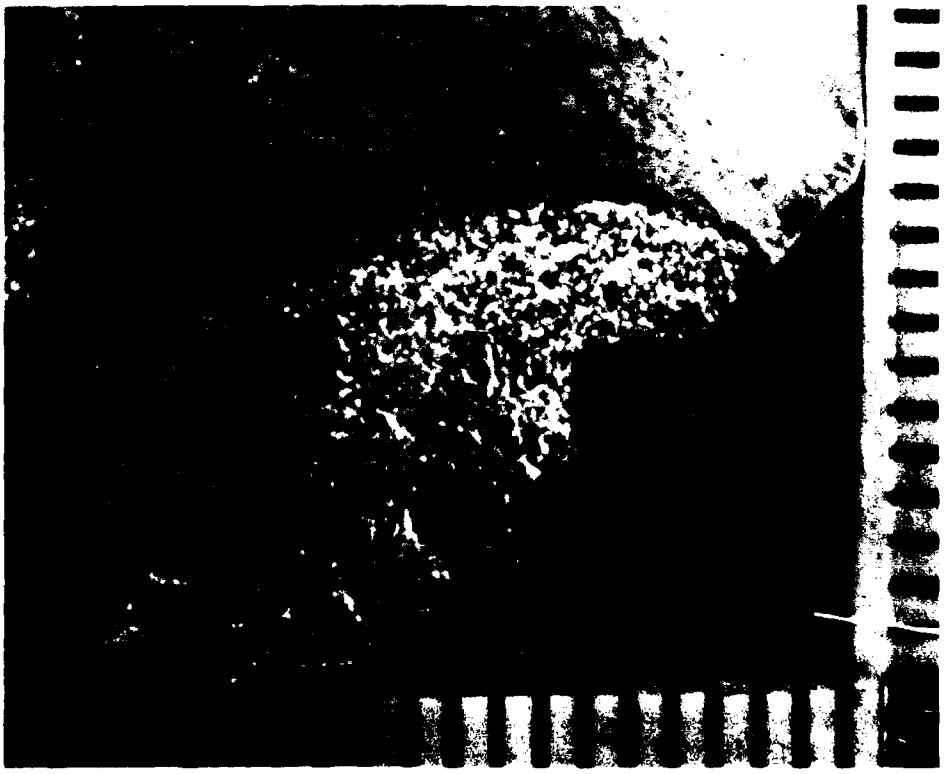

← Radius → →| |← 0.01-inch

(b) Specimen number 1B

Figure 3-5. Enlarged photographs of fractures from surface flawed specimens

(a) Specimen number 2A

← Radius →

(b) Specimen number 2B

Figure 3-6. Enlarged photographs of fractures from corner flawed specimens

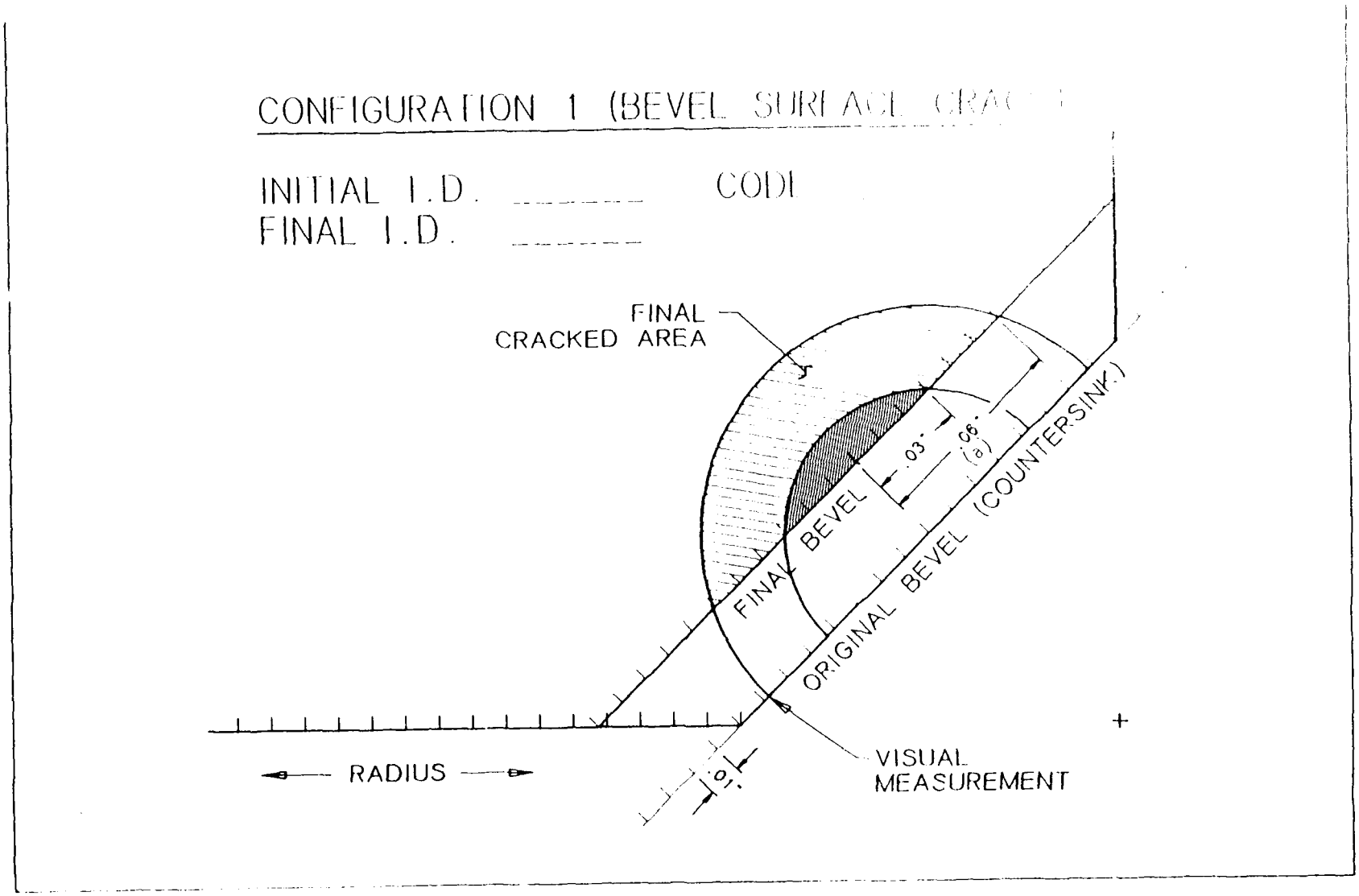

Figure 3-7. Illustration of technique for estimating final surface crack lengths

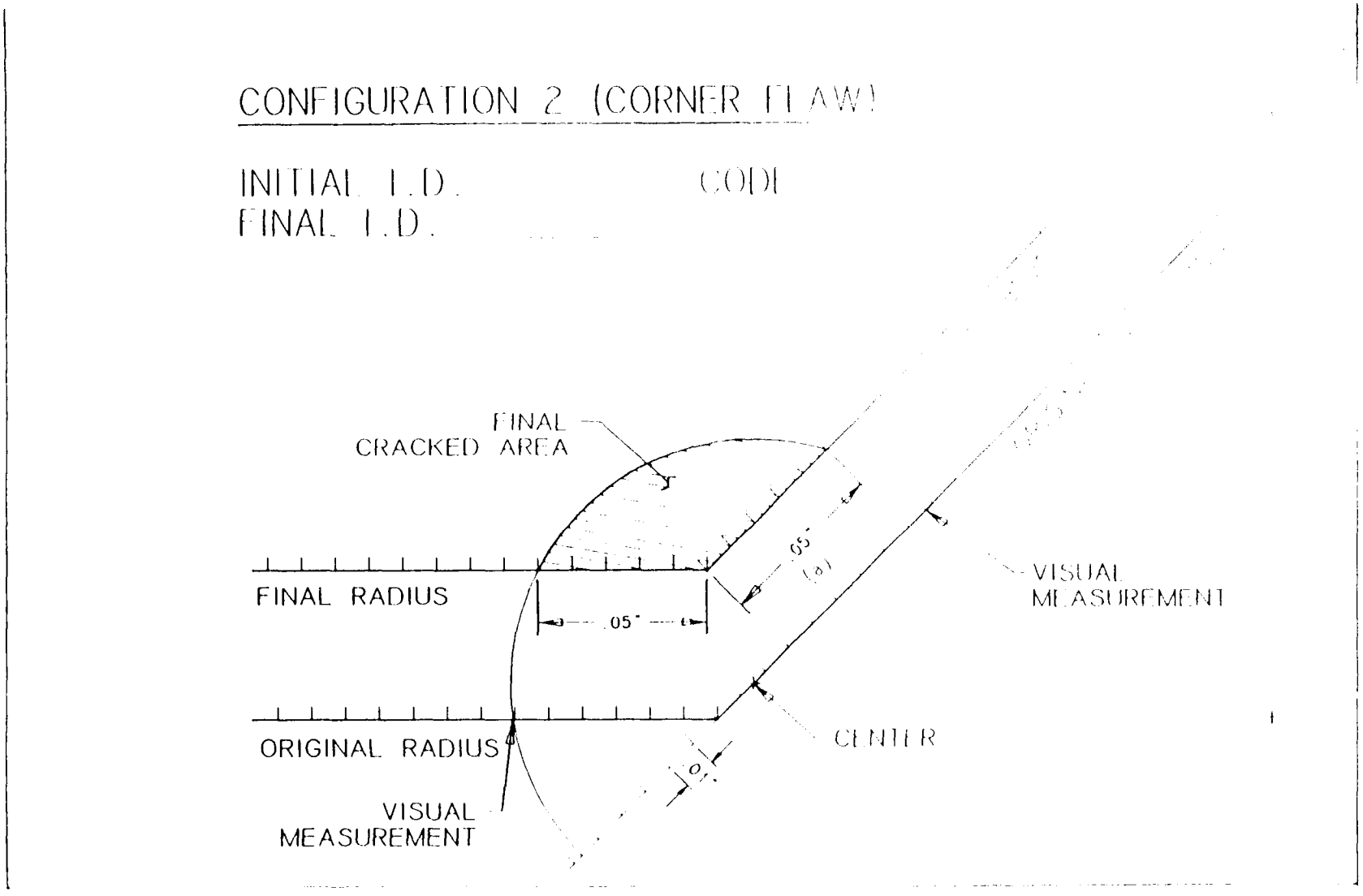

Figure 3-8. Illustration of technique for estimating final corner crack lengths

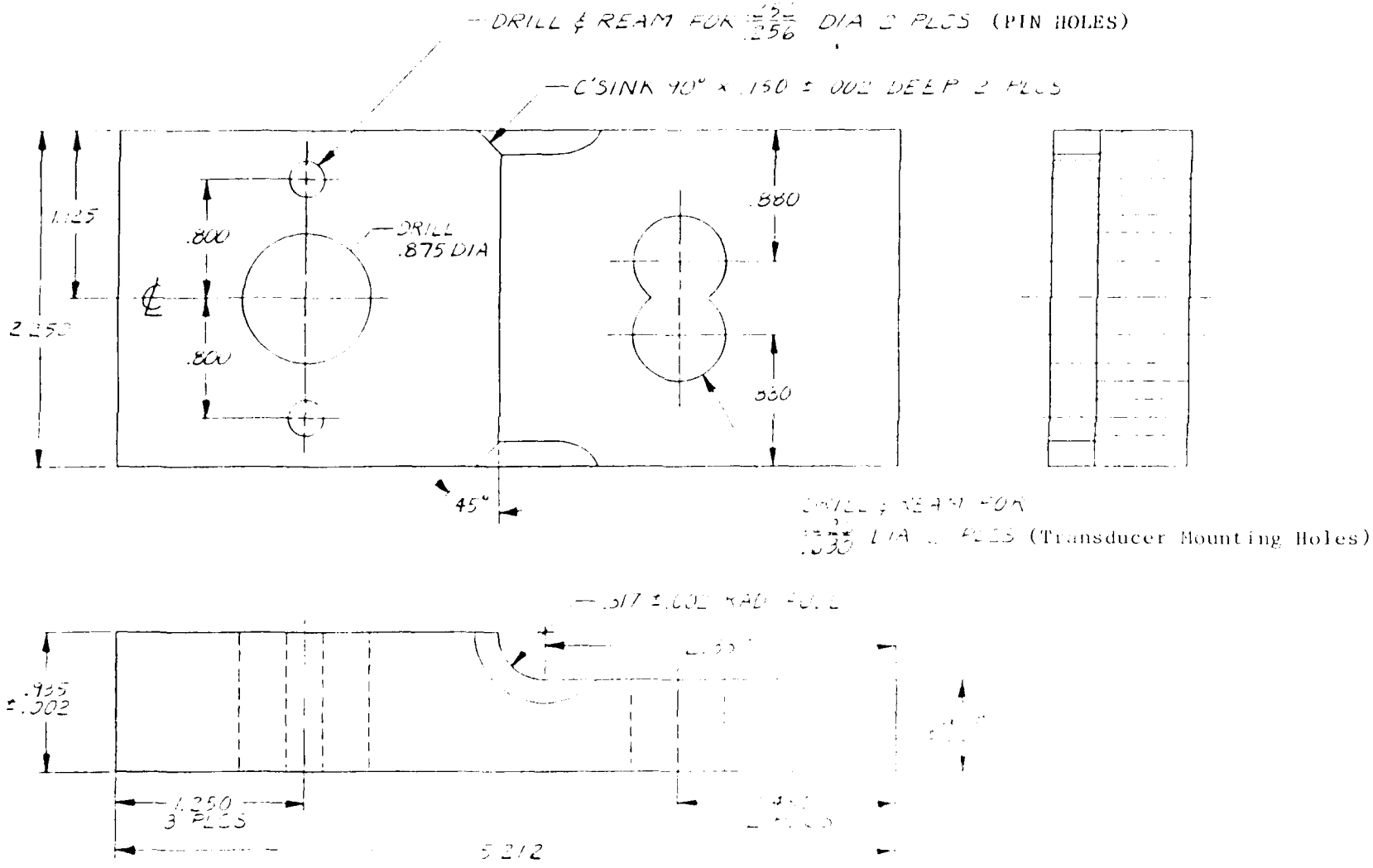

Figure 3-9. Final design for all test specimens

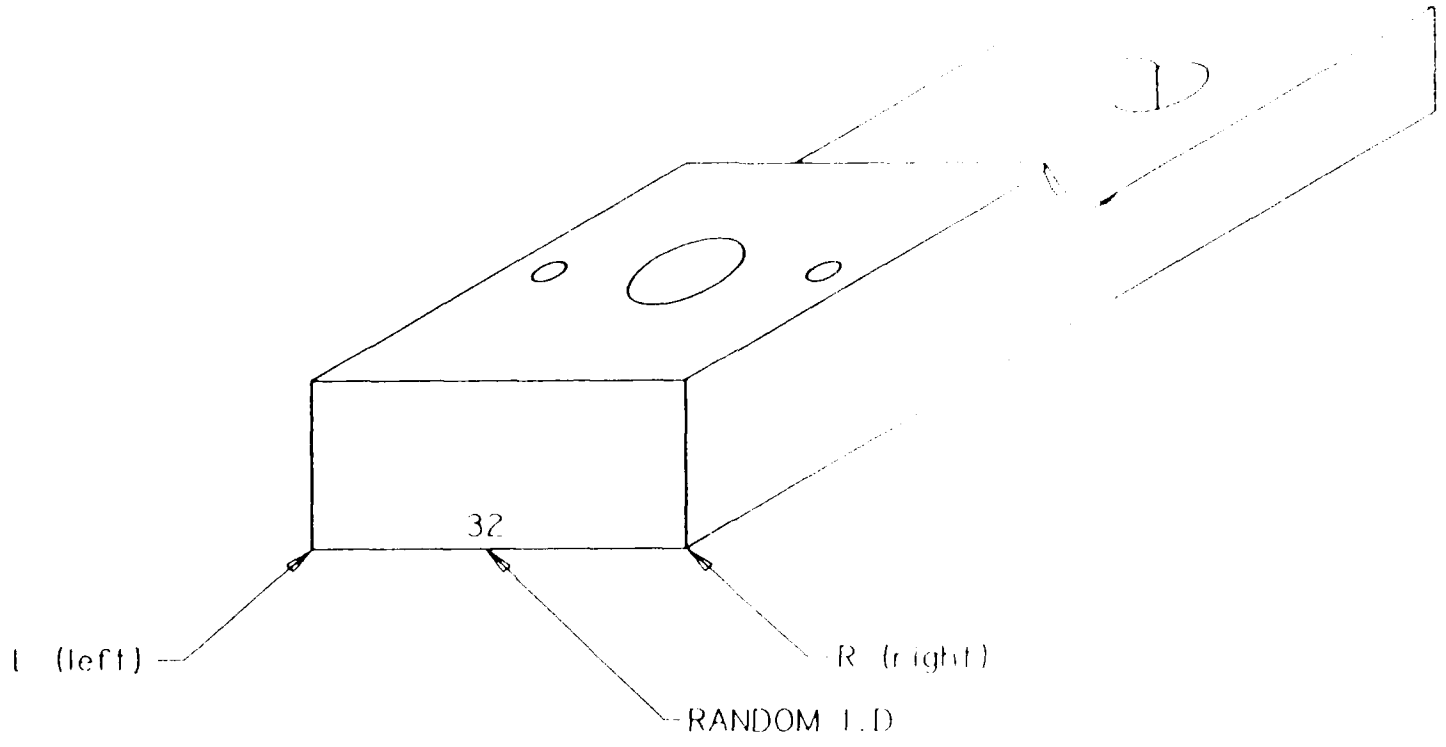

Figure 3-10. Viewing orientation of specimen for determining right and left sides

4. STATISTICAL ANALYSIS OF FLAW INSPECTION DATA

4.1 Sample Size Determination

The number of flawed and unflawed specimens needed in this study was determined using the concept of binomial statistics. The flaw detection process used in the reliability testing required only a "yes" or "no" result; i.e., a crack was detected or it was not detected. The sample size selected was consistent with the reliability and confidence level stated in the project Statement of Work: a sample size of 29 flawed specimens was needed to maintain 95-percent confidence with 90-percent POD (1). The same number of unflawed specimens was needed to estimate the reliability of the detection technique with no flaws present. Section 4.2 details the specific number of flawed/unflawed specimens.

4.2 Inspection Summary

Four inspectors were assigned the task of inspecting the same set of flawed and unflawed specimens. The set consisted of 69 specimen surfaces with no flaws, 34 specimen surfaces with corner cracks, and 31 specimen surfaces with surface cracks. These were combined to form 67 simulated lugs, each with two inspection surfaces for the purposes of this analysis. Each "lug" could contain zero, one, or two flaws. Table 4-1 summarizes the flaws and approximate crack sizes, by category, used in this study. The flaw size referred to in this table and used in the statistical analysis is that estimated from the procedures described in the previous section. For surface cracks, the estimated size is one-half of the estimated surface length; for corner cracks, the size is the length of the crack on the countersink (bevel) surface. As previously discussed, the crack depth was smaller than would be expected if the crack shape was formed by a true radius equal to half the flaw surface length.

All four inspectors correctly identified 63 of the 65 specimen surfaces which contained flaws. All flaws in the 0.06- to 0.04-inch range were found by every inspector. The two flaws that were not detected by the four inspectors were in the lower flaw size range. Their estimated sizes were 0.029 and 0.0315 inch, but they were later found to be much smaller (Section 4.5). Additionally, three of the four inspectors accurately identified all 69 unflawed specimen surfaces as having no flaws. However, one inspector did conclude that a flaw existed on two unflawed specimen surfaces. A summary of the inspection results is outlined in Table 4-2.

Table 4-1

POD STUDY SPECIMEN DATA SUMMARY

Type of Specimen	Estimated Flaw Size, a (inch)*	Number of Locations
Unflawed	-	69
Corner crack	0.03	5
Corner crack	0.04	9
Corner crack	0.05	15
Corner crack	0.06	5
Surface crack	0.03	5
Surface crack	0.04	7
Surface crack	0.05	15
Surface crack	0.06	4

Table 4-2

INSPECTION ERRORS BY INSPECTOR

Inspector	Flaw Type	Specimen No.	Estimated Flaw Size, a (inch)*	Results
A	Surface	32L	0.0290	Missed
A	Surface	69R	0.0315	Missed
B	Surface	32L	0.0290	Missed
B	Surface	69R	0.0315	Missed
B	Unflawed	14L	--	Detected
B	Unflawed	93L	--	Detected
C	Surface	32L	0.0290	Missed
C	Surface	69R	0.0315	Missed
D	Surface	32L	0.0290	Missed
D	Surface	69R	0.0315	Missed

*The flaw sizes are the estimated half-lengths, a, as shown in Figures 3-7 and 3-8.

4.3 Reliability of Detecting 0.050-Inch Flaws

Since all four inspectors were able to detect all 30 of the 0.050-inch range flaws accurately, the POD of 90 percent of the 0.050-inch fatigue cracks at a 95-percent confidence level was exceeded. Thus, the inspection capability exceeds the reliability requirements in the 0.050-inch crack range.

4.4 Probability of Detection Curves

Additional analysis of the inspection data yielded POD curves which represent the probability of detecting a flaw at a given flaw size, a. The primary purpose of this analysis was to extend the POD determination to smaller flaw sizes than the target size of *0.050 inch*. Inspection processes that result in only a "yes" or "no" output can be depicted by POD curves using a binomial grouping method or a maximum likelihood method.

4.4.1 Binomial Grouping Analysis

The binomial grouping analysis used to generate POD curves utilizes the concept of moving averages (2). This is achieved by collecting a large number of cracks with varying sizes, grouping them into clusters whose size is comparable to the detection capability of the inspection process, recording the resultant inspection outcome at each flaw, and plotting the probability of detection for each cluster versus the median flaw size in the cluster. This method is appropriate if a large number of flaws are available covering a wide range of crack sizes.

Since the data in this study resulted in only two flaws that were not detected, the binomial grouping analysis was not appropriate to use in calculating a POD curve. This method employs regression techniques to model the POD function as it is related to flaw size. Only five of the 37 clusters calculated in this data set had POD values that were not 100 percent. Therefore, regression techniques could not appropriately model the POD curve with so few data points other than 100 percent.

4.4.2 Maximum Likelihood Analysis

The maximum likelihood analysis method is more commonly used than the binomial grouping method because it does not require a clustering of the data. It is based on the log-logistic function of the POD curve. This function is

$$POD(a) = \frac{e^{\alpha+\beta ln(a)}}{1+e^{\alpha+\beta ln(a)}}$$

The parameters α and β can be estimated by the method of maximum likelihood (3). The crack size is designated by a. This method uses the "yes" and "no" information from the detection process and estimates the parameters α and β so that they maximize the probability for obtaining the observed data by solving the following simultaneous equations

$$0 = \sum_{i=1}^{N} n_i p_i - \sum_{i=1}^{N} \frac{n_i e^{\alpha+\beta ln(a_i)}}{1+e^{\alpha+\beta ln(a_i)}} \quad (1)$$

$$0 = \sum_{i=1}^{N} n_i p_i ln(a_i) - \sum_{i=1}^{N} \frac{n_i ln(a_i) e^{\alpha+\beta ln(a_i)}}{1+e^{\alpha+\beta ln(a_i)}} \quad (2)$$

These equations allow results from several inspections of the flawed specimens to be used in the calculation of the POD curve. P_i equals the proportion of times the ith crack was detected by the four inspectors. For example, if the first crack were found by all four inspectors, then p_i would be 1.0. If the first crack were detected by three of the four inspectors, then p_i would be 0.75. N_i represents the number of times the ith crack was inspected; a_i, the crack radius; and N, the total number of cracks inspected.

The inspection data gathered in this study were processed by using the maximum likelihood technique, and the resulting POD curve is illustrated in Figure 4-1. Using log-logistic modeling, the probability of detection for a 0.050-inch crack is 97.9 percent.

There are some underlying problems associated with probability of detection modeling techniques in analyzing the data collected in this study. First, maximum likelihood estimates are commonly used when inspection results are gathered in the form of yes/no type data. If multiple inspections of each flaw are collected, the number of inspections has a significant impact on the POD modeling and the resultant confidence bounds on the POD curve. It has been suggested that at least ten inspections per crack be collected in a multiple inspection study (4). This criterion will allow better estimates of the probability of detection of an individual crack size. With fewer inspections, as in this study, there is a greater probability that the estimates will only be 1 or 0; i.e., either each inspection results in a detection or each inspection results in a missed crack. This problem is primarily a result of the success of the inspection. The study was originally designed to ensure a 95-percent confidence level for 0.050-inch flaws.

Since the data analyzed for this detection study had only four inspections per flaw, the POD model illustrated in Figure 4-1 is not very stable. It has a poor statistical fit since the data do not fit a log-logistic model with high accuracy. Additionally, the model is being influenced greatly by the two flaws that were missed by all four inspectors. These two flaws, coupled with the small number of inspections, lead to lower confidence bound estimates that are extremely wide.

This strengthens the fact that the POD model used to extend the analysis to smaller flaw sizes is unstable and, therefore, should be viewed with caution.

In order to evaluate how the lower confidence bounds are affected by the two "missed" flaws at the lower end of the crack size scale, a model was determined from the data without these two flaws. This step is justified because these missed flaws were much shorter and shallower than estimated (see Section 4.5). Figure 4-2 illustrates a 95-percent lower confidence bound on the probability of detection curve. There are two important points to note in this model. First, the POD curve is close to 1.0 for all crack sizes; however, extrapolation of POD estimates for cracks less than 0.028 is not recommended since data were not taken in that range. Second, caution should be used in the interpretation of the confidence bounds since the sample sizes of the flaws in the 0.030- to 0.045-inch range are small. The 95-percent lower confidence bound at the 0.050-inch crack is 97 percent.

4.5 Comparison of Estimated Crack Length and Actual Crack Length

The fabrication of the flawed specimens resulted in an "estimate" of the crack length used in the statistical analysis. To determine the accuracy of the crack length estimates, several flaws were broken open and measured. The results are shown in Table 4-3. It was concluded that of the cracks inspected by this method, all were smaller in depth than estimated (also see Table 3-2); thus, all had depths much smaller than half of the surface length. Four of the measured corner cracks were longer in the countersink surface than estimated, but the maximum underestimate was only 0.004 inch, or 13 percent, whereas the depths of these cracks were less than the estimated size by 23 to 50 percent. Therefore, the interfacial area of the cracks (one common estimate of eddy current flaw amplitude response) was significantly smaller than the area calculated using estimated crack size.

The two flaws that were missed by all inspectors could not be measured for depth, indicating that they were extremely shallow. Considering length alone, however, they would still be only 0.017 and 0.016 inch in size. Therefore, the POD curves computed in Section 4.2.2 are conservative; resulting POD curves from the actual crack lengths, if calculated, would be shifted to the left in Figures 4-1 and 4-2. Thus, the POD for a 0.050-inch crack would be greater than 97.9 percent.

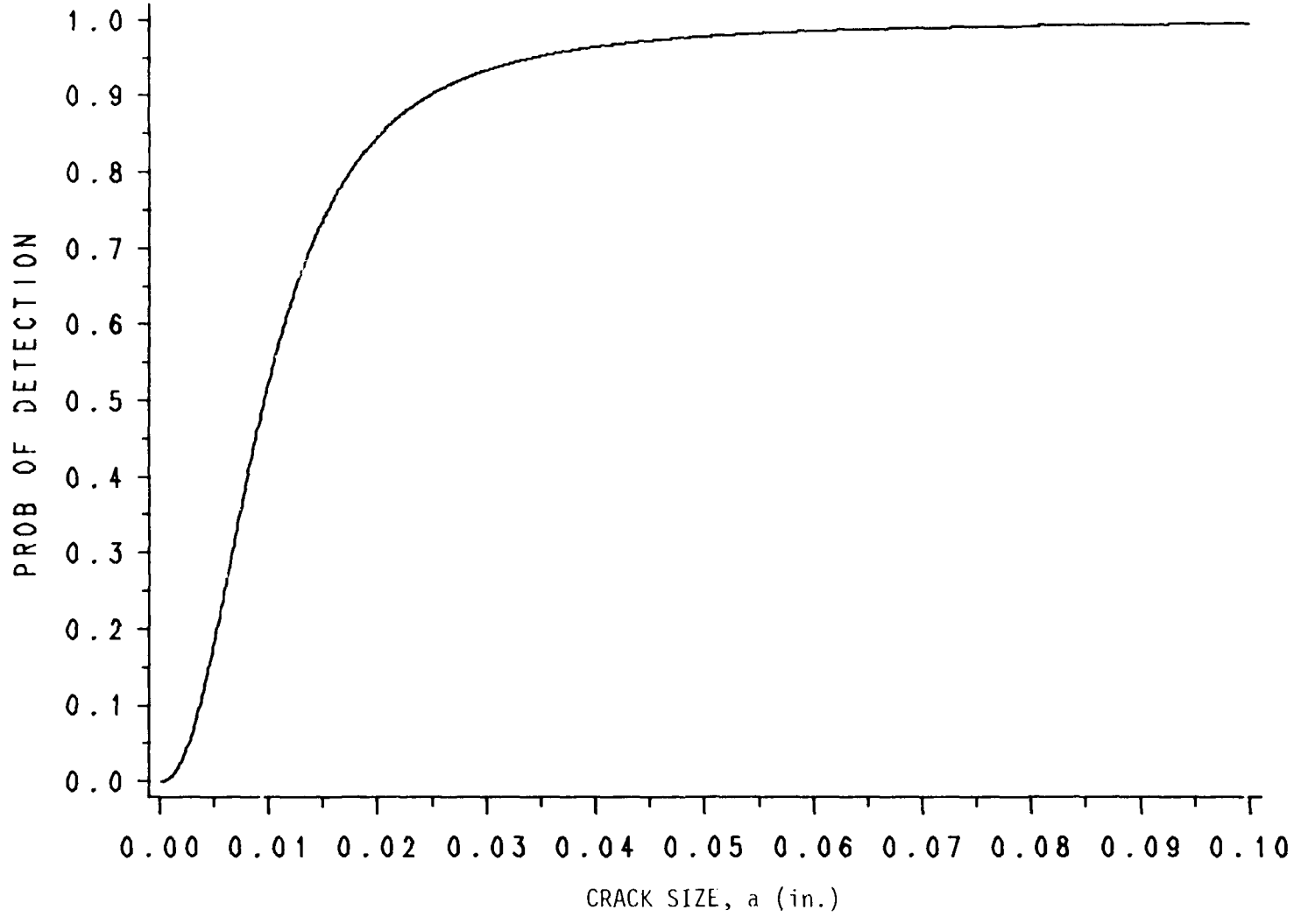

Figure 4-1. POD results using the maximum likelihood method. The results are conservative since the estimated size used in the calculations is known to overestimate actual crack surface length and depth, as discussed in Section 4.5.

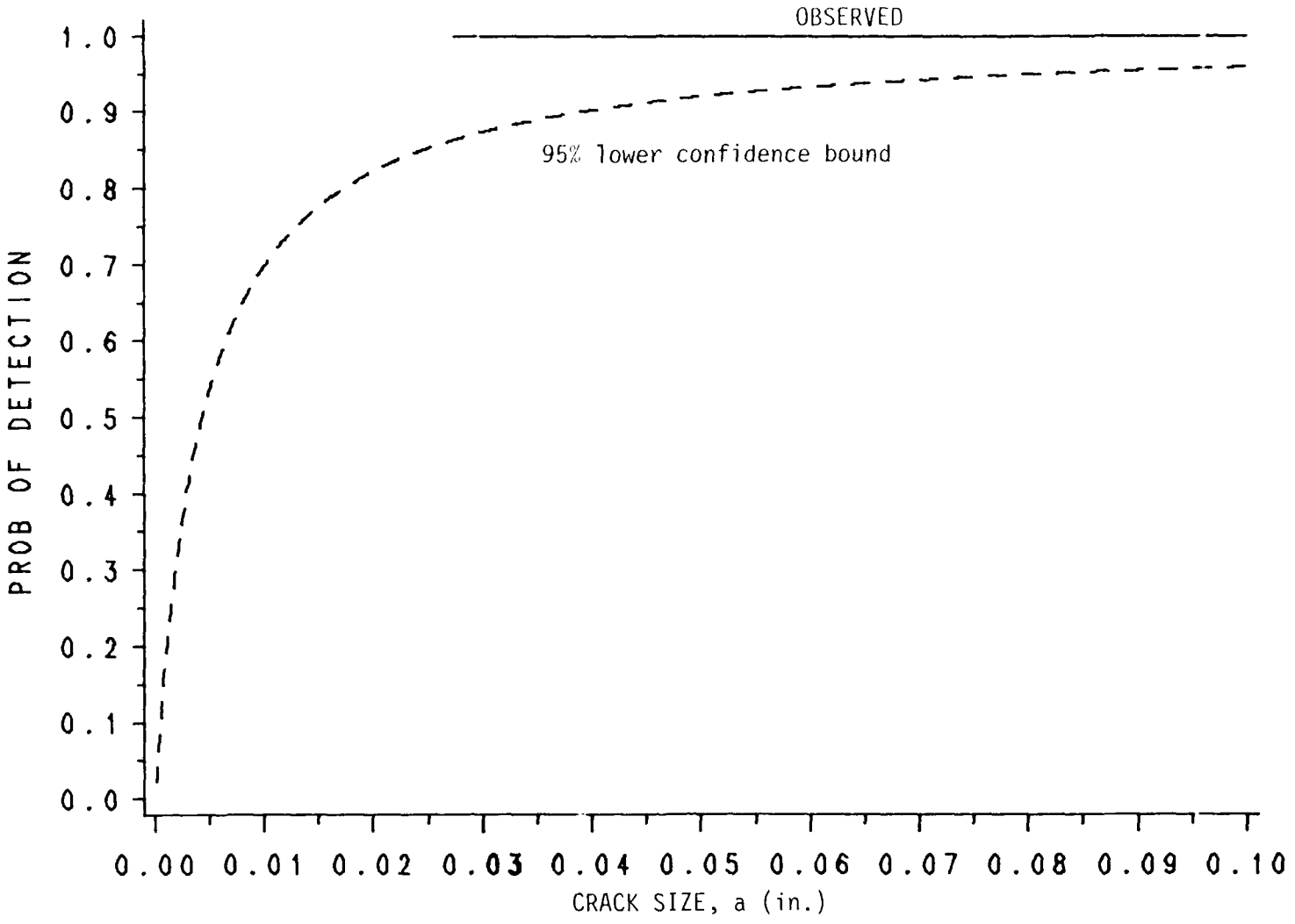

Figure 4-2. POD results with the two flaws of unmeasurable (extremely small) depths removed from the calculations. The results are conservative since the estimated size used in the calculations is known to overestimate actual crack surface length and depth, as discussed in Section 4.5.

Table 4-3

ESTIMATED VERSUS MEASURED CRACK PARAMETERS

Surface Cracks

Spec. I.D.	Estimated Crack Size (inch)	Actual Crack Half-Length (inch)	Maximum Actual Depth (inch)	Difference Estimated/Actual Half-Length (inch)
32	0.029	0.017	*	-0.012
50	0.030	0.022	0.006	-0.008
63	0.033	0.030	0.013	-0.003
69	0.032	0.016	*	-0.016
72	0.033	0.025	0.007	-0.008
37	0.055	0.047	0.021	-0.008
38	0.055	0.047	0.019	-0.008
46	0.050	0.049	0.025	-0.001

*Broke outside of flaw when pulled to failure

Corner Cracks

Spec I.D.	Estimated Crack Length (inch)		Actual Crack Length (inch)		Actual Depth (inch)*	Difference Estimated/ Actual Length (inch)	
	Countersink	Radius	Countersink	Radius		Countersink	Radius
18	0.028	0.026	0.022	0.022	0.013	-0.006	-0.004
80	0.036	0.030	0.040	0.022	0.019	+0.004	-0.008
91	0.031	0.033	0.035	0.010	0.018	+0.004	-0.023
25	0.055	0.040	0.056	0.030	0.031	+0.001	-0.010
27	0.052	0.040	0.055	0.030	0.027	+0.003	-0.010
41	0.056	0.049	0.059	0.028	0.023	+0.003	-0.021

*Depth was measured along the bisector of the angle between the radius and countersink surfaces.

5. CONCLUSION

The initial goal of developing and qualifying an inspection technique for the lug geometry was met, and the actual inspection performance goals were exceeded; the 95-percent lower confidence bound on the POD is greater than 92 percent for 0.050-inch size cracks and greater than 90 percent for 0.038-inch size cracks. Furthermore, these numbers are known to be conservative because the actual crack depths are estimated to be only 0.031 inch for 0.050-inch size cracks and 0.023 inch for 0.038-inch size cracks.

This performance in a difficult geometry was possible through (1) redesign of the lug geometry to provide a uniform, inspectable surface, and (2) use of a mechanical manipulator device to guide the probe. The results show that a high inspection reliability can be achieved in field inspections, if significant effort is made in personnel selection, technique development, training, and followup support. It is believed that this approach to inspection development can be used in other critical regions to reduce the amount of inspections required by reducing the detectable flaw size.

6. REFERENCES

1. Owen, D. B., *Handbook of Statistical Tables*, Reading, Massachusetts: Addison-Wesley Publishing Company, Inc., 1962, pp. 317-318.

2. Rummel, W. D., Christner, B. K., Mullen, S. J., and Long, D. L., *Characterization of Structural Assessment Testing*, SA-ALC/MMEI/1/86, January 1986.

3. Rummel, W. D., Christner, B. K., and Long, D. L., "Methodology for Analysis and Characterization of Nondestructive Inspection Capability Data," *Review of Progress in Quantitative Nondestructive Evaluation, 7B*, Plenum Press, New York, 1987, pp.1769-1776.

4. Berens, A. P., and Hovey, P. W., *Flaw Detection Reliability Criteria, Volume I - Methods and Results*, AFWAL-TR-84-4022, April 1984.

APPENDIX

PROCEDURE FOR THE EDDY CURRENT INSPECTION OF T-37 LOWER SPAR CAP LUGS

SwRI Project No. 17-7958

Prepared for

SA-ALC/MMEI
Kelly Air Force Base
San Antonio, Texas 78241-5000

Prepared by

Department of NDE Science and Research
Nondestructive Evaluation Science and Technology

January 1989

T-37 FRONT WING SPAR, LOWER CAP LUG INSPECTION PROCEDURE

1. PURPOSE

The purpose of this inspection is to detect surface-breaking flaws in the T-37 front wing spar, lower cap lug critical surfaces using eddy current testing (ET) methods.

2. SCOPE

This procedure provides the information and detailed steps necessary for inspection for surface-breaking cracks in the lower cap lugs in the areas shown in Figure 1. The inspection surfaces have been machined to provide for an improved inspection reliability.

3. EQUIPMENT

3.1 NORTEC NDT-19 ET instrument

3.2 Remote-control cable for the NDT-19 [Southwest Research Institute (SwRI) part No. 7958-851-56)]

3.3 T-37 lug inspection device (SwRI part No. 7958-851-300)

3.4 Probe adapter cable (SwRI part No. 7958-851-101)

3.5 *Differential shielded eddy current probe (SwRI part No. 7958-300)*

3.6 Panasonic video recorder AG-2400 and Sharp 570S microphone

3.7 Calibration fixture (SwRI part No. 7958-70317) and standard (SwRI part No. 7958-851)

3.8 Professional-grade VHS-T-120 video-tape cartridge (Ampex part No. 189-T-120-6a or equivalent)

3.9 Audio headphones

3.10 Panasonic monitor (Panasonic part No. 930) and cabling

4. PERSONNEL

4.1 The personnel performing this inspection shall be certified Level III based on the requirements of MIL-STD-410D.

4.2 Additionally, personnel performing this inspection shall have been trained in this procedure by a Level III certified individual experienced in this procedure.

5. DOCUMENTS

5.1. NDT-19 instrument operation manual

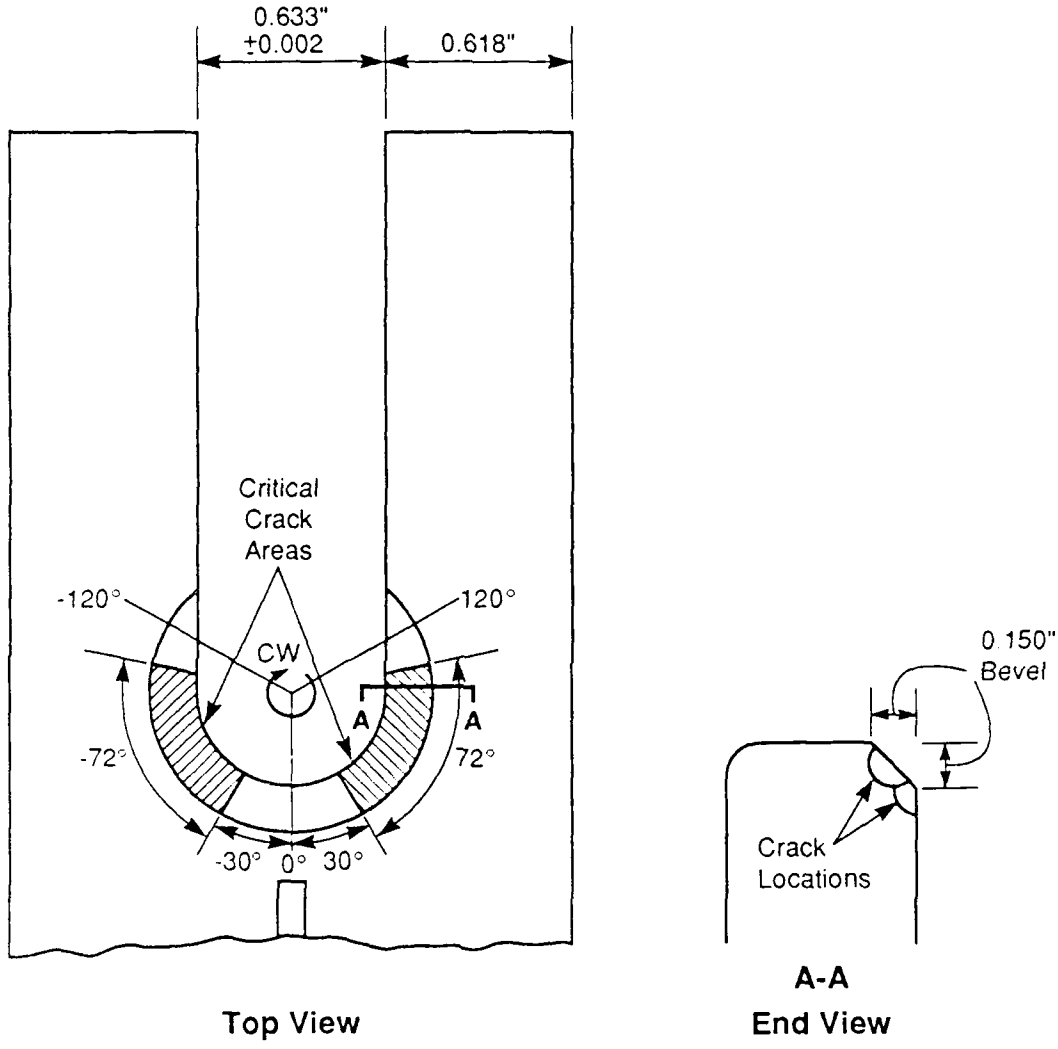

No Scale

Note: The exam area is from +120° to -120° in a clockwise direction.
The critical crack areas have a higher probability of flaw generation.

Figure 1. Examination areas

5.2 VCR operator manual

6. CALIBRATION

6.1 A calibration will be performed immediately before the inspection of each lug.

6.2 A calibration check will be performed

(1) At any time the operation of the equipment is in question and

(2) At the end of the inspection of each lug.

6.3 The calibration standard has four simulated inspection surfaces (shown in Figure 2) which are as follows:

(1) Surface 1, containing three flaws produced by electrodischarge machining (EDM) in the center of the machined surface with radii of 0.030, 0.040, and 0.050 inch.

(2) Surface 2, containing three EDM flaws at the inner radius of the machined surface with radii of 0.030, 0.040, and 0.050 inch, as shown in Figure 2.

(3) Surface 3, containing no flaws.

(4) Surface 4, which has an irregular surface representative of improper machining.

7. EQUIPMENT SETUP

7.1 Mechanical

7.1.1 Check probe head and cam assembly for foreign material in the probe manipulator shown in Figure 3. Dirt or other particles can be removed with an aerosol solvent/lubricant spray such as WD-40.

7.1.2 Ensure that the screws are tight on the spring attachment and that the probe is returned to the bottom of the slot by spring tension after being manually retracted.

CAUTION: DEVICE DAMAGE MAY RESULT IF THE FOLLOWING STEP IS OMITTED.

7.1.3 Check that the radial position knob is at zero degrees on the pointer when the probe is pointing directly away from the probe manipulator body. If the probe is at any other angle, check the Allen screw or radial positioning knob. It this is firmly engaged into the shaft, then the unit must be repaired and is not suitable for use.

CAUTION: DEVICE DAMAGE MAY RESULT IF THE FOLLOWING STEP IS OMITTED.

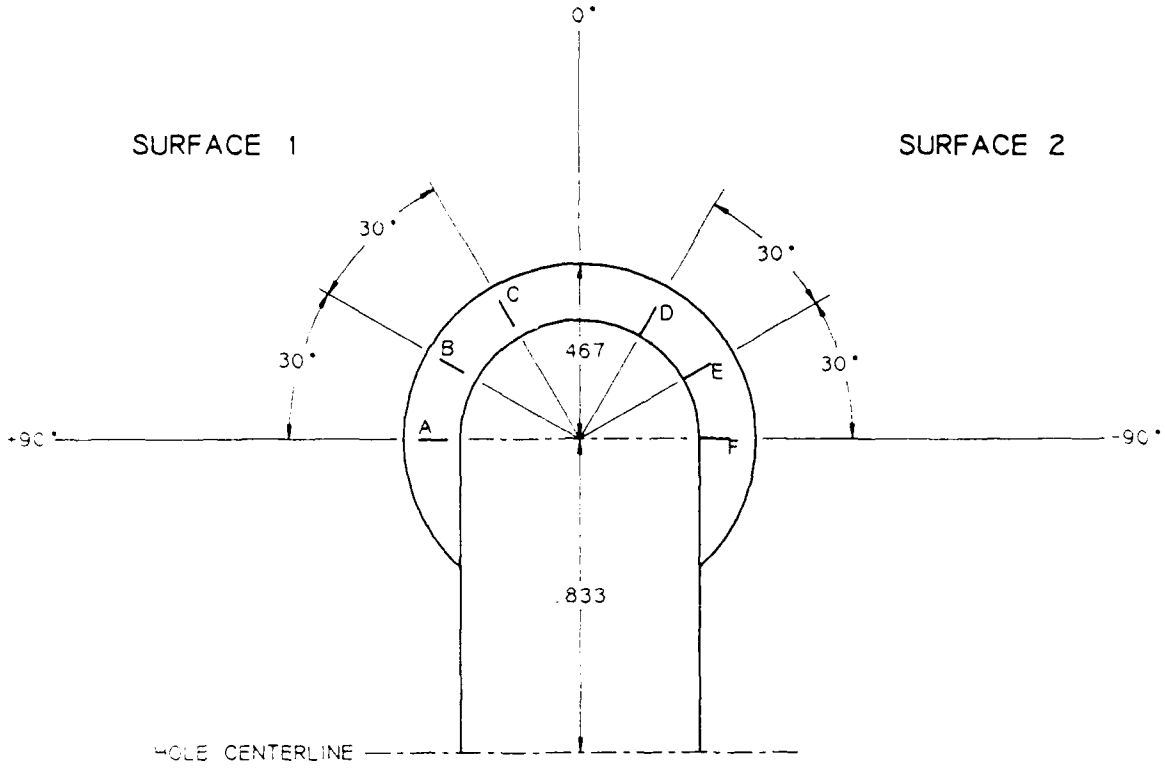

TOP VIEW SHOWING SURFACES 1 AND 2

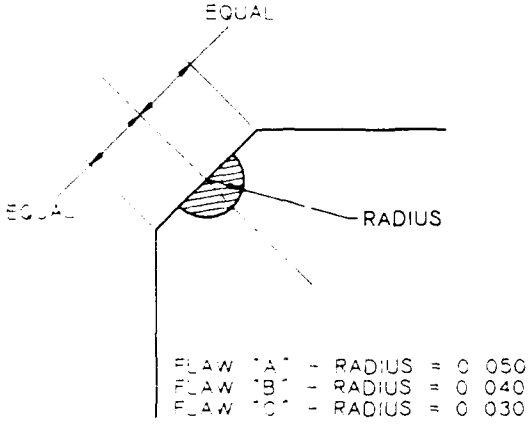

FLAWS "A", "B", "C"

SIDE VIEW OF SURFACE 1

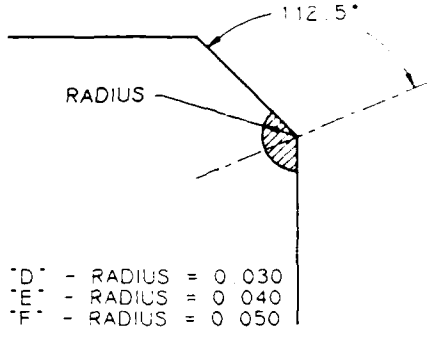

FLAWS "D", "E", "F"

SIDE VIEW OF SURFACE 2

Figure 2a. Calibration standard illustrating Surfaces 1 and 2

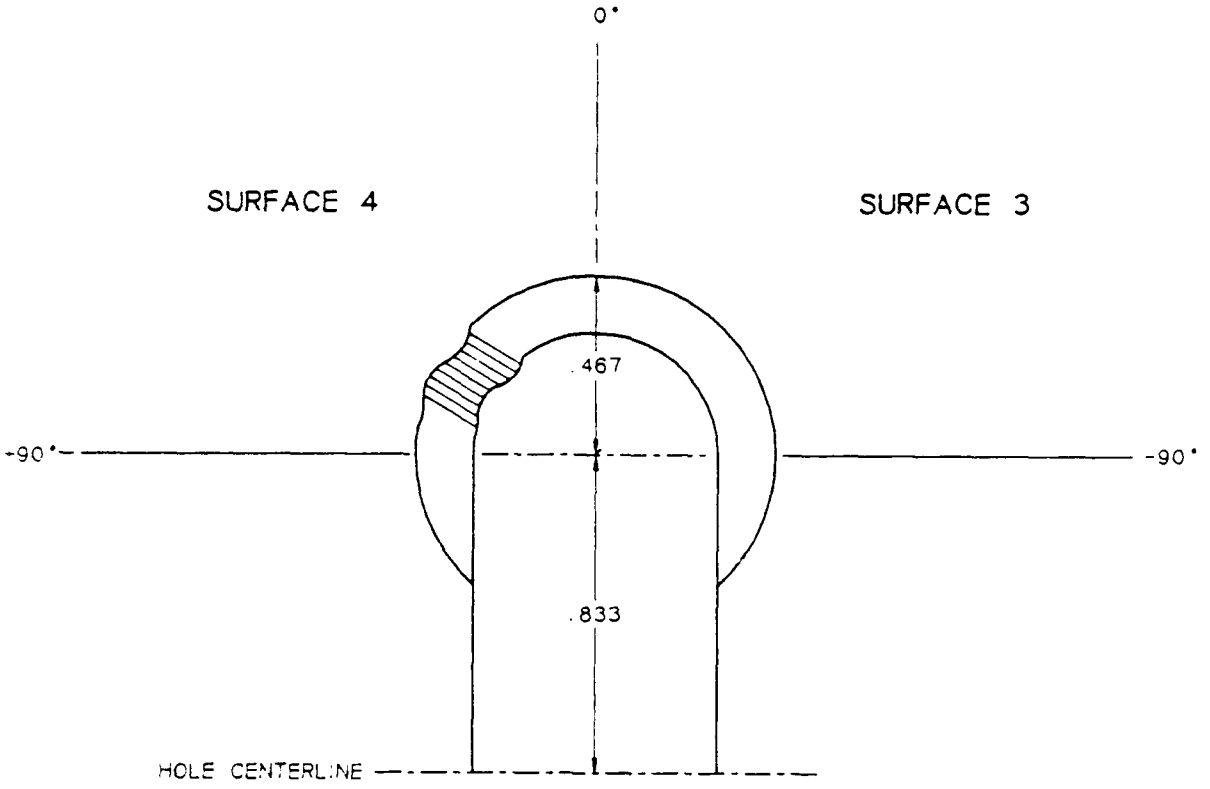

TOP VIEW SHOWING SURFACES 3 AND 4

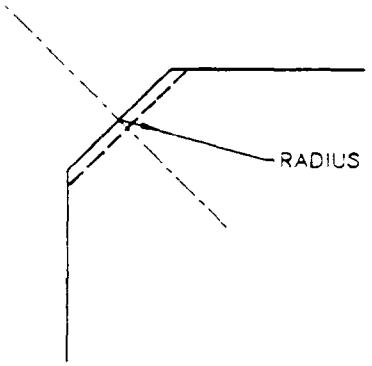

SIDE VIEW OF SURFACE 4

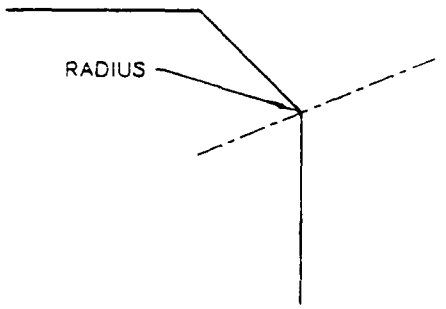

SIDE VIEW OF SURFACE 3

Figure 2b. Calibration standard illustrating Surfaces 3 and 4. Note: Surface 3 does not contain flaws, and Surface 4 is representative of improper machining.

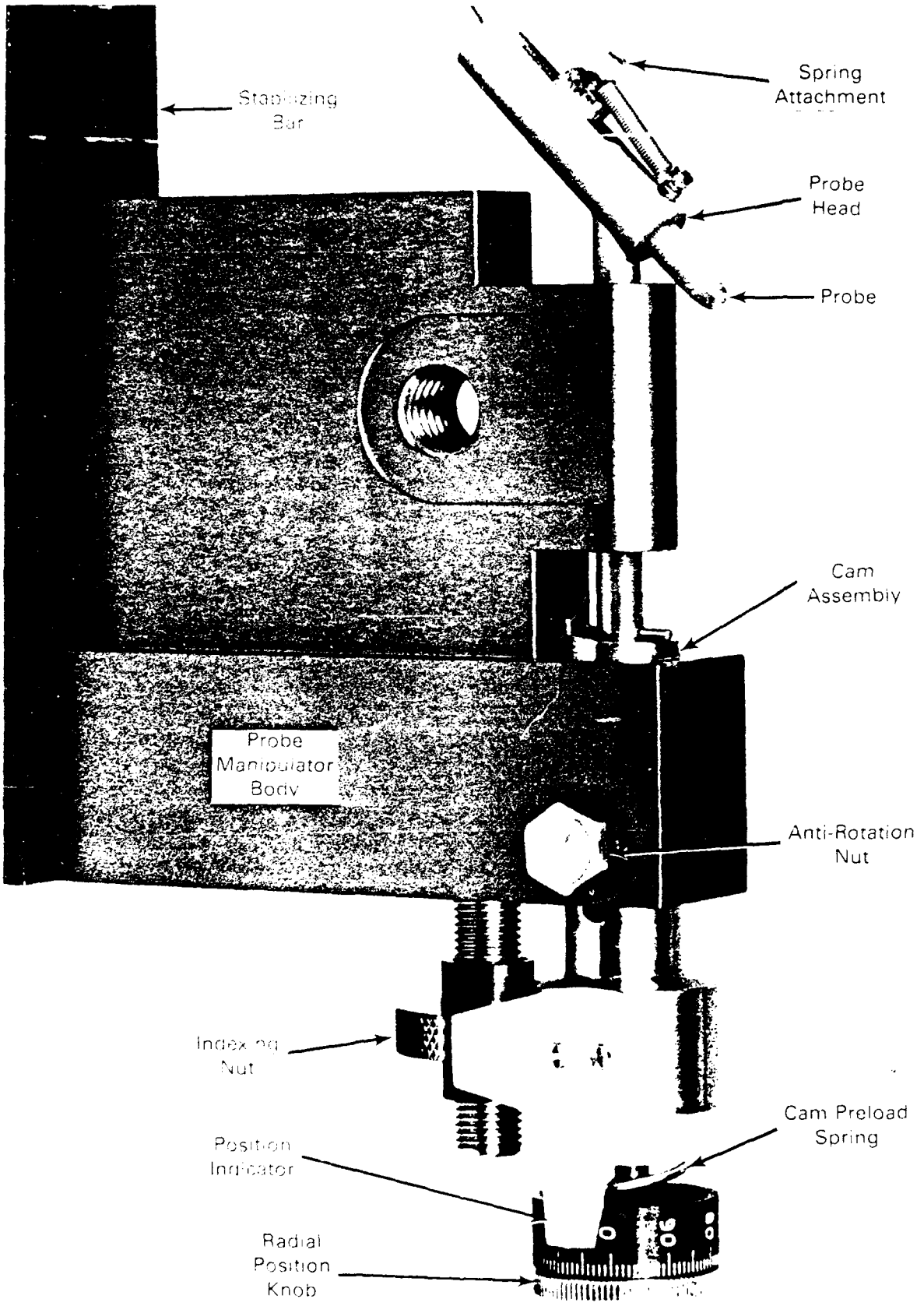

Figure 3. Photograph of the inspection device

7.1.4 Rotate the indexing nut until the cam assembly is flush against the probe manipulator housing. This ensures that the probe is off the surface as it is inserted into the lug.

7.1.5 Attach the stabilizing bar to the probe manipulator and upper attachment plate, as shown in Figure 4. Tighten the bolts firmly with your fingers. This assembly constitutes the inspection device.

7.1.6 Set up the calibration fixture so that the probe can be scanned over surfaces 1 and 2.

7.1.7 Place the inspection device into the calibration fixture and place the shoulder bolts in place, as shown in Figure 4.

7.1.8 Tighten the bolts attaching the stabilizing bar to the probe manipulator and upper attachment plate. This step ensures that the inspection device is aligned with the wing hole centerline.

7.1.9 Insert the shoulder bolts in the probe manipulator and upper attachment plate and hand tighten firmly, thus completing the mechanical assembly and setup of the inspection device.

7.2 Cabling (Refer to Figure 5 for the system diagram)

7.2.1 Connect the probe adaptor cable (SwRI part No. 7958-851-101) to the front of the ET instrument terminal marked "Probe."

7.2.2 Connect the probe (SwRI part No. 7958-300) to the adaptor cable identified in step 7.2.1.

7.2.3 Connect the remote-control cable (SwRI part No. 7958-851-56) to the back of the instrument at the terminal marked "I/O." Place remote null and balance controls on the floor within easy reach of your feet during the inspection.

7.2.4 Connect the VCR video input to the ET instrument video output using the remote control cable (SwRI part No. 7958-851-56) attached in Step 7.2.3.

7.2.5 Connect the microphone and headphones to the VCR.

7.2.6 Connect the Panasonic-monitor video input to the VCR video output.

7.2.7 Turn on the VCR , ET instrument, and monitor. Insert the tape.

7.2.8 Zero the tape counter, and set the speed to "SP."

7.2.9 Place the VCR into the record mode.

7.2.10 Start the VCR, and count backwards from ten to one into the microphone. Stop the VCR.

7.2.11 Rewind the tape.

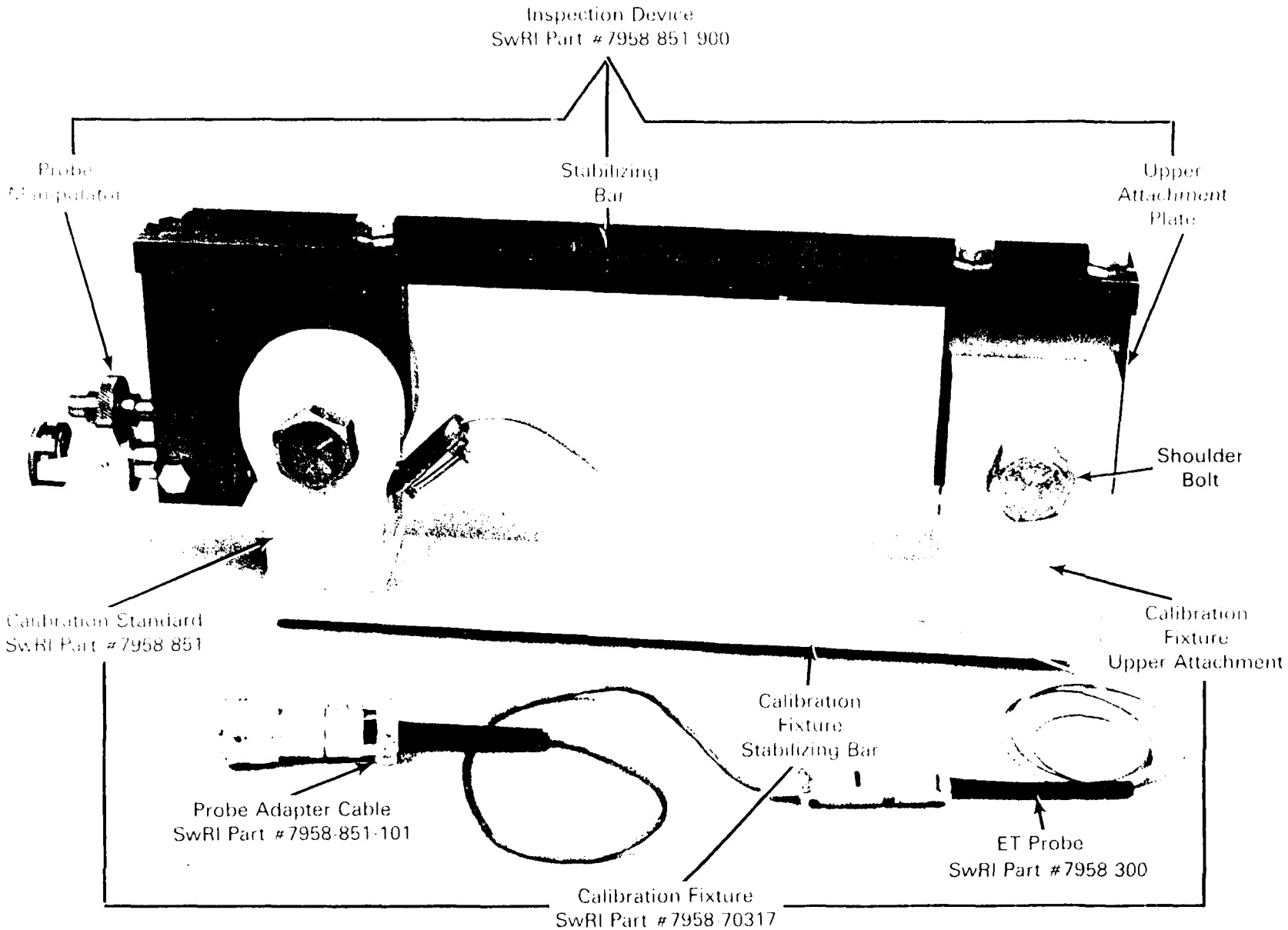

Figure 4. Inspection device installed in calibration fixture

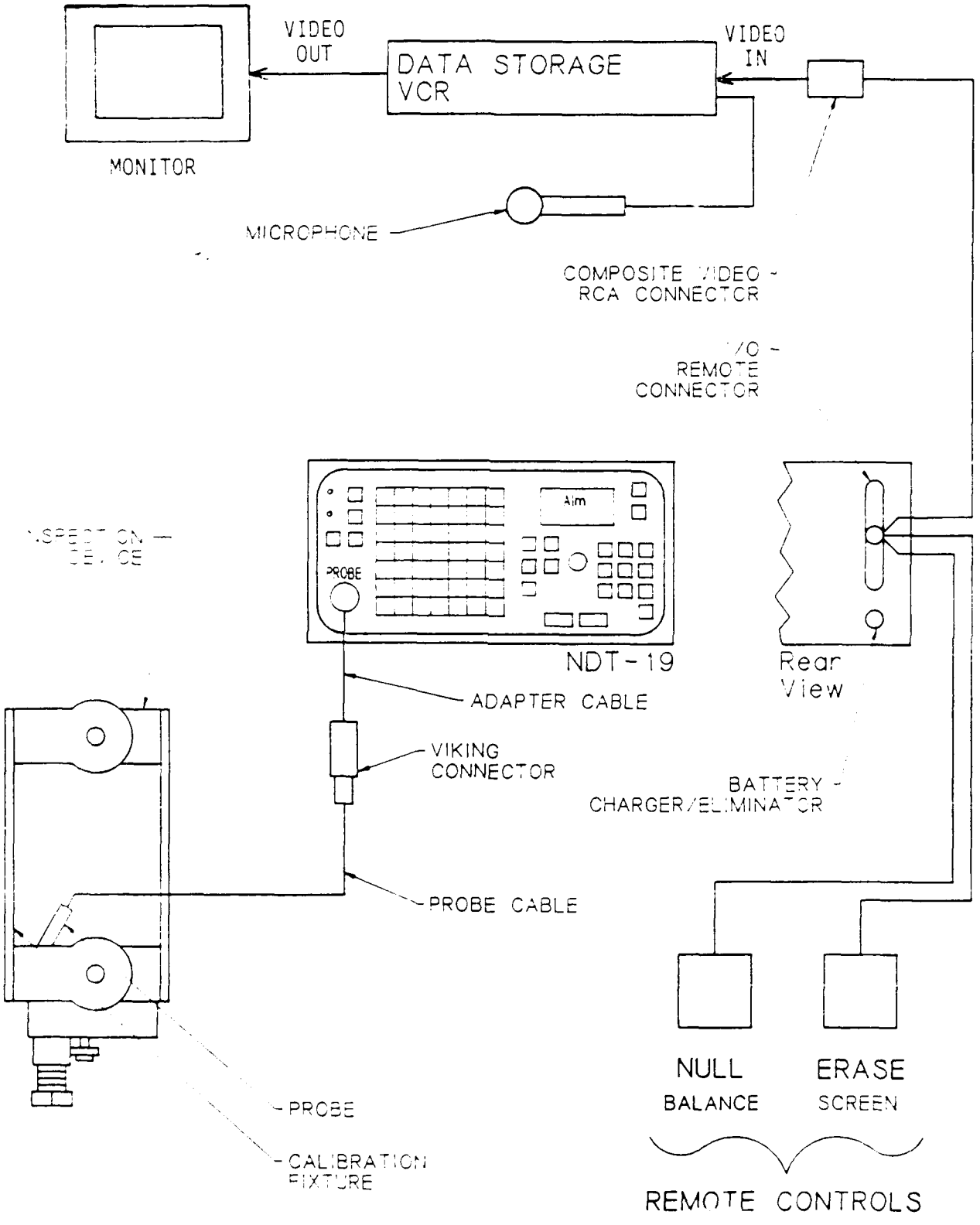

Figure 5. Inspection system assembly diagram

7.2.12 Press the PLAY control, and verify that the audio has been recorded by listening on the tape or headphone. If no audio has been recorded, check the VCR and microphone. Also, look at the monitor; if the grid pattern is not present when the tape is replayed, then check the cable connections and VCR.

7.2.13 Rewind the tape.

7.3 Instrument Setup and Calibration

7.3.1 Allow 5 minutes for instrument warm-up before performing any actual inspections or calibrations.

7.3.2 Set frequency No. 1 at 300 KHz and frequency No. 2 to the OFF position.

7.3.3 Set the gain initially to 70 for vertical and 60 for horizontal channels.

7.3.4 Set the erase mode to manual.

7.3.5 Set the balance mode to continuous null.

7.3.6 Make sure the probe drive is set to HIGH.

7.3.7 Set the high-pass filter at 0 and the low-pass filter at 100.

7.3.8 Turn the sweep mode to OFF.

7.3.9 Balance the instrument by depressing the NULL control on instrument or foot pedal.

7.3.10 Erase the screen.

7.3.11 If the dot is visible and at the center of the CRT, go to step 7.3.13. If not, check the screen position control (POSN). Set Position Vertical and Position Horizontal to 128. This step is necessary, since the dot can be positioned off the screen. If no dot is visible, decrease the gain, and rebalance the instrument. If no dot is visible, remove the probe connector, and rebalance. If there is still no dot visible after all of these steps, substitute another instrument, and begin at step 6.2.1.

7.3.12 If the dot is visible after removal of probe connector, substitute a replacement adapter cable and probe and rebalance the instrument. If the dot reappears, then try the original adapter cable; if the dot no longer appears, then the adapter cable is defective. If upon substituting the original probe, the dot does not appear, then the original probe is defective.

NOTE: FAILURE TO ACCOMPLISH STEPS 7.3.13, 7.3.14, AND 7.3.16 WILL RESULT IN EXTREME SETUP ERROR. ENSURE THAT THE GAIN IS SET PROPERLY AS PER 7.3.3.

7.3.13 Set the probe radial position to 0 degrees. Adjust the indexing nut to bring the probe to the center of the bevel surface.

7.3.14 Balance the instrument, then pull the probe back from the surface using the spring attachment screw. Observe the direction of the dot on the screen. Using the phase-angle adjustment, rotate the vector so that the pattern generated by the probe liftoff is down from the center of the screen approximately 10 degrees to the left of the vertical screen center line. This is the liftoff vector, as shown in Figure 6.

7.3.15 Rotate the radial position knob back and forth approximately 60 degrees on the dial to get the signal generated by changes in the angle of the probe to the surface. This pattern should be symmetric about the origin in the horizontal plane. A slight adjustment of the phase-angle control might be necessary to put the pattern into the horizontal plane. This operation is critical, since the majority of the noise generated during the inspection is in this direction. The pattern is the tilt vector, as shown in Figure 6.

7.3.16 Rotate the manipulator to pass the center of the probe over the three notches in the center of the bevel at surface 1. Three characteristic eddy current figure-eight flaw patterns will be generated, as shown in Figure 7.

7.3.17 Adjust the gain of the instrument until the magnitude of the vertical component of the signal pattern from the 0.050-inch flaw is 6 ±.5 vertical screen divisions. ***It is important*** to adjust the gain proportionally to maintain the same phase relationships. If gain changes are required, refer to the gain table shown in Figure 8. The values in the gain table should correspond to the nearest 0.5 dB of the instrument settings. The instrument must be rebalanced after each change in gain. The pattern from the 0.050-inch flaw will be at a 40- to 50-degree angle. Shallow surface scratches or tool marks will be in the horizontal plane.

7.3.18 Check the phase angle of the tilt and liftoff signals using the method described in steps 7.2.13 and 7.2.14. Note the phase angle of these two signals.

7.3.19 Turn on the alarm gate by depressing the ALM button, as described in the manual in Section 4. Define a positive alarm gate so that when the dot passes into the gate the alarm is triggered. Gate settings are shown in Figure 6. Note that the purpose of the alarm gate is to assist in the detection of flaws. Analysis is based on pattern characteristics.

> NOTE: IF A FLAW INDICATION DOES NOT BREAK THE ALARM GATE, IT COULD STILL BE A FLAW. THE MAGNITUDE OF THE VECTOR IS NOT TO BE CONSIDERED SIGNIFICANT IN EVALUATION OF THE FLAW SIGNAL.

7.3.20 Set the alarm gate boundaries by using the SP 01 command and the arrow and number key pad (as described in the manual) to occupy the quadrants shown in Figure 6.

7.3.21 Verify that the figure-eight flaw pattern generated by the dot over the shallowest flaw in surface 1 triggers the alarm gate. If the alarm is not triggered, check the instrument gain and probe position. Also compare the observed flaw pattern to the typical calibration signal pattern shown in Figure 7.

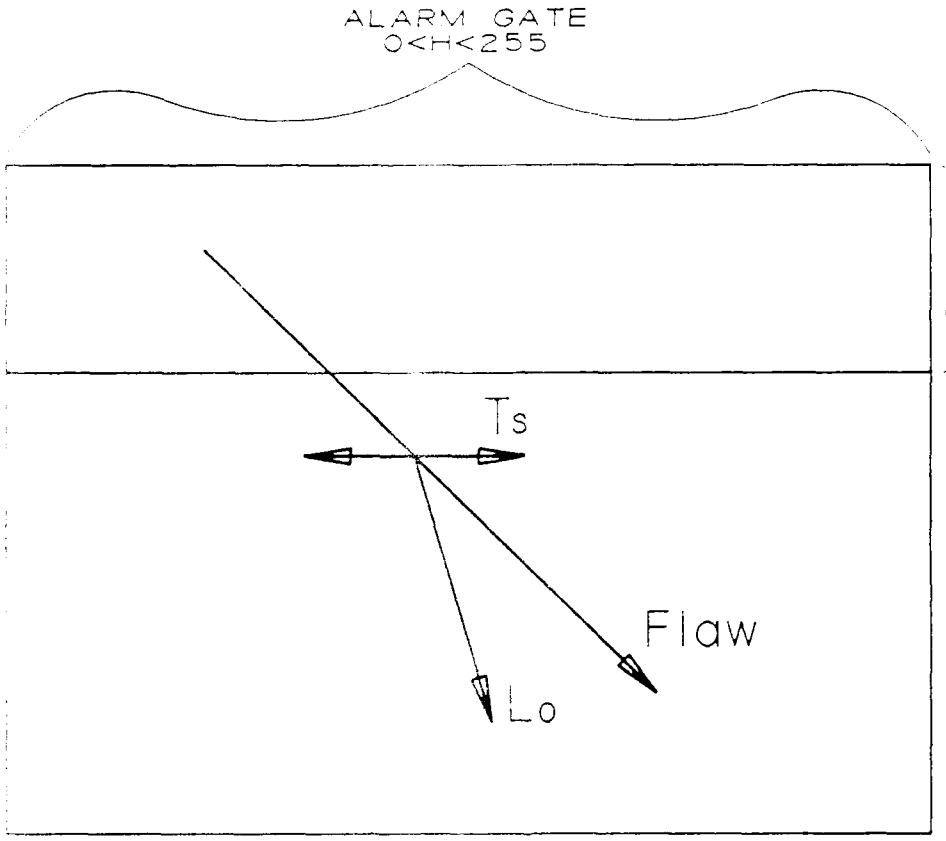

Lo = LIFTOFF VECTOR

Ts = SURFACE NOISE OR TILT VECTOR

Flaw = FLAW VECTOR
TYPICAL OF FLAWS WITH SOME DEPTH

Figure [illegible] Impedance plane vector diagram

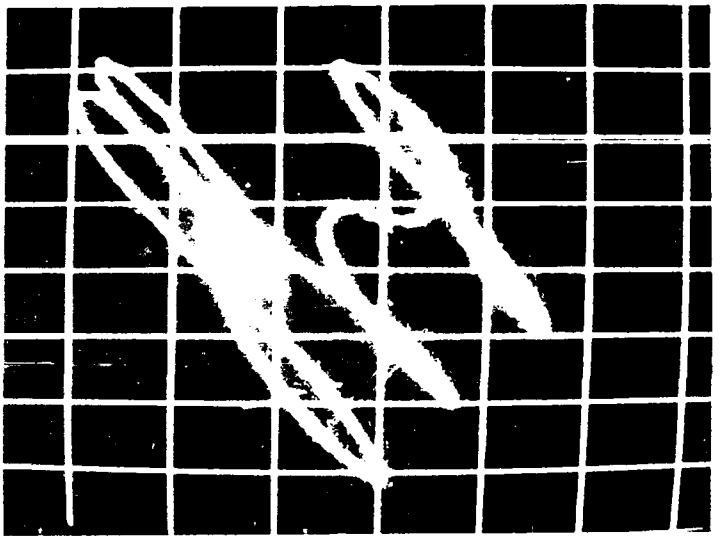

Figure-eight flaw patterns generated by the 0.030-, 0.040-, and 0.050-inch deep EDM notches in calibration surface 1

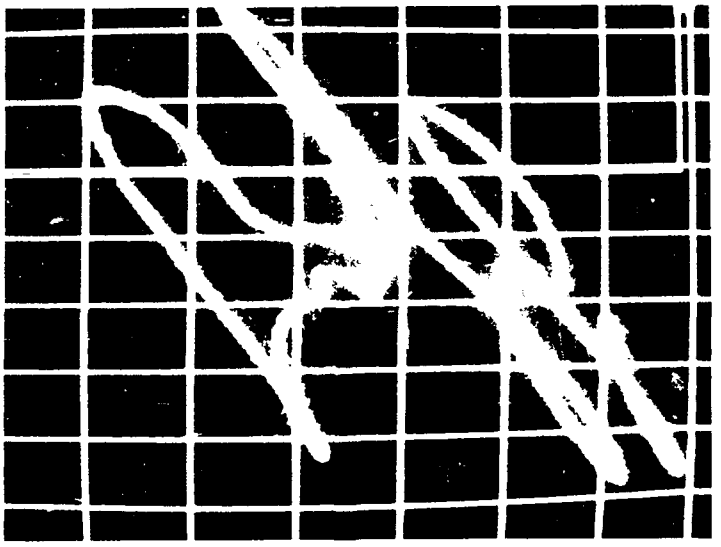

Figure-eight flaw pattern generated by the 0.030-, 0.040-, and 0.050-inch deep EDM notches in calibration surface 2

Figure 7. EDM notch signals

GAIN TABLE

Horizontal	Vertical	Horizontal	Vertical
[illegible]	0.00	40.00	46.67
[illegible]	1.17	41.00	47.83
[illegible]	2.33	42.00	49.00
[illegible]	3.50	43.00	50.17
[illegible]	[illegible]	44.00	51.33
[illegible]	[illegible]	45.00	52.50
[illegible]	[illegible]	[illegible]	53.67
[illegible]	[illegible]	[illegible]	54.83
[illegible]	[illegible]	[illegible]	56.00
[illegible]	[illegible]	[illegible]	57.17
[illegible]	[illegible]	[illegible]	58.33
[illegible]	[illegible]	[illegible]	59.50
[illegible]	[illegible]	[illegible]	60.67
[illegible]	[illegible]	[illegible]	61.83
[illegible]	[illegible]	[illegible]	63.00
[illegible]	[illegible]	56.00	65.33
[illegible]	[illegible]	57.00	66.50
[illegible]	[illegible]	59.00	68.83
[illegible]	[illegible]	60.00	70.00
[illegible]	[illegible]	61.00	71.17
[illegible]	[illegible]	[illegible]	72.33
[illegible]	[illegible]	[illegible]	73.50
[illegible]	[illegible]	[illegible]	74.67
[illegible]	[illegible]	[illegible]	75.83
[illegible]	[illegible]	66.00	77.00
[illegible]	[illegible]	67.00	78.17
[illegible]	[illegible]	68.00	79.33
[illegible]	[illegible]	69.00	80.50
[illegible]	[illegible]	70.00	81.67
[illegible]	[illegible]	[illegible]	82.83
[illegible]	[illegible]	72.00	84.00
[illegible]	[illegible]	73.00	85.17
[illegible]	[illegible]	74.00	86.33
[illegible]	[illegible]	75.00	87.50
[illegible]	[illegible]	76.00	88.67
[illegible]	[illegible]	[illegible]	89.83

Note: NDT-1 [illegible] dB.

[illegible] Gain table

7.3.22 Record all instrument settings, time, and tape counter on calibration and inspection record form NDT-9 and audibly on the VCR. Record one pass over calibration surface 1 on the VCR along with a description of the flaws on the audio track.

7.3.23 Rotate the indexing nut to position the lower edge of the probe at the lower edge of the bevel at the 0-degree radial position. Record one pass over calibration surface 2 on the VCR along with a description of the flaws on the audio track.

7.3.24 Rotate the indexing nut until it is flush against the housing.

7.3.25 Rotate the radial position knob to zero.

7.3.26 Remove the inspection device from the calibration fixture. Remove the calibration standard, and replace it after it has been rotated [illegible] degrees so that surfaces 3 and 4 are available to the probe.

7.3.27 Install the inspection device into the calibration fixture [illegible] 7.1.3 through 7.1.7 and 7.1.9.

7.3.28 Scan the probe over surface 3 and the unflawed regions for determining the background noise from the inspection area. Record on the [illegible] on the audio track.

7.3.29 Scan surface 4, which represents improperly machined surfaces. Note the phase angle of the noise from this surface as the probe tilt angle is [illegible] vary. If the instrument is set up properly, the signals from surface [illegible] to go off the screen. Record on the VCR, and identify on the audio track. This concludes the calibration of the inspection device and instrument. [illegible] of the aircraft.

8. INSPECTION PROCEDURE

8.1 Install the inspection device on the wing to be inspected, as described [illegible] through 7.1.7 and 7.1.9.

8.2 Using the indexing nut, adjust the probe vertical position to the [illegible] surface (top edge of the probe at the top edge of the bevel). [illegible] indexing nut causes 0.041 inch in vertical travel. Approximately [illegible] required to complete all scans of the bevel.

8.3 Set the radial position dial so that it aligns with the pointer at the [illegible]

8.4 Balance the instrument.

8.5 Record the aircraft and wing number on the calibration and [illegible] tape cartridge. Start the VCR; and record the start time of the [illegible] wing number, and aircraft tail number.

8.6 Prepare for the scan by rotating the scanning knob counter [illegible] toward the inspection surface) to the mechanical stop. Then [illegible] by **slowly** rotating clockwise to the other stop. Observe the [illegible]

figure-eight flaw pattern noted during calibration is generated, then it must be considered to be a flaw indication. (Refer to section 9 for further analysis.) If an audible alarm is generated, rescan the region at a slower speed, and pay careful attention to the signal pattern. If a figure-eight pattern is generated, refer to section 9. If a pattern is generated similar to that from surface 4 as noted during calibration, the surface may be too rough for proper examination.

NOTE: IMPROPER MACHINING CAN CAUSE SIGNIFICANT NOISE LEVELS. TOOL MARKS, CHATTER, AND SCRATCHES SHOULD BE BROUGHT TO THE ATTENTION OF THE PERSONNEL PERFORMING THE MACHINING FOR CORRECTIVE ACTION.

[illegible] IS ACCOMPLISHED, THE [illegible] BE COMPLETELY REINSPECTED.

8.7 [illegible]

8.8 [illegible]

8.9 [illegible] scan number on the audio track.

8.10 Repeat the scanning procedure described in step 8.6 while data are recorded in the VCR.

8.11 After indexing the probe four times, observe the location of the probe. Inspect the part until the [illegible] edge of the probe overlaps the corner of the bevel throughout the critical area defined in Figure 1.

NOTE: THIS MAY REQUIRE MORE THAN FOUR COMPLETE SCANS. THE INDEXING UNIT WILL PROBABLY HAVE TO BE ADJUSTED A PARTIAL REVOLUTION TO ACHIEVE THE REQUIRED PROBE OVERLAP.

8.12 Remove inspection device as per steps 7.1.3 - 7.1.5.

8.13 Install inspection device into calibration fixture [illegible]

8.14 Perform [illegible]

9. DATA ANALYSIS

9.1 Part [illegible] with a phase angle and shape similar to the calibration figure-eight flaw pattern must be considered to be cracks.

9.2 The [illegible] pattern as a function of the probe position over the flaw is shown in Figure [illegible]. This is due to the variation in the flaw signal caused by geometry and the [illegible] over the maximum flaw depth.

9.3 [illegible] is not to be [illegible] flaw signal

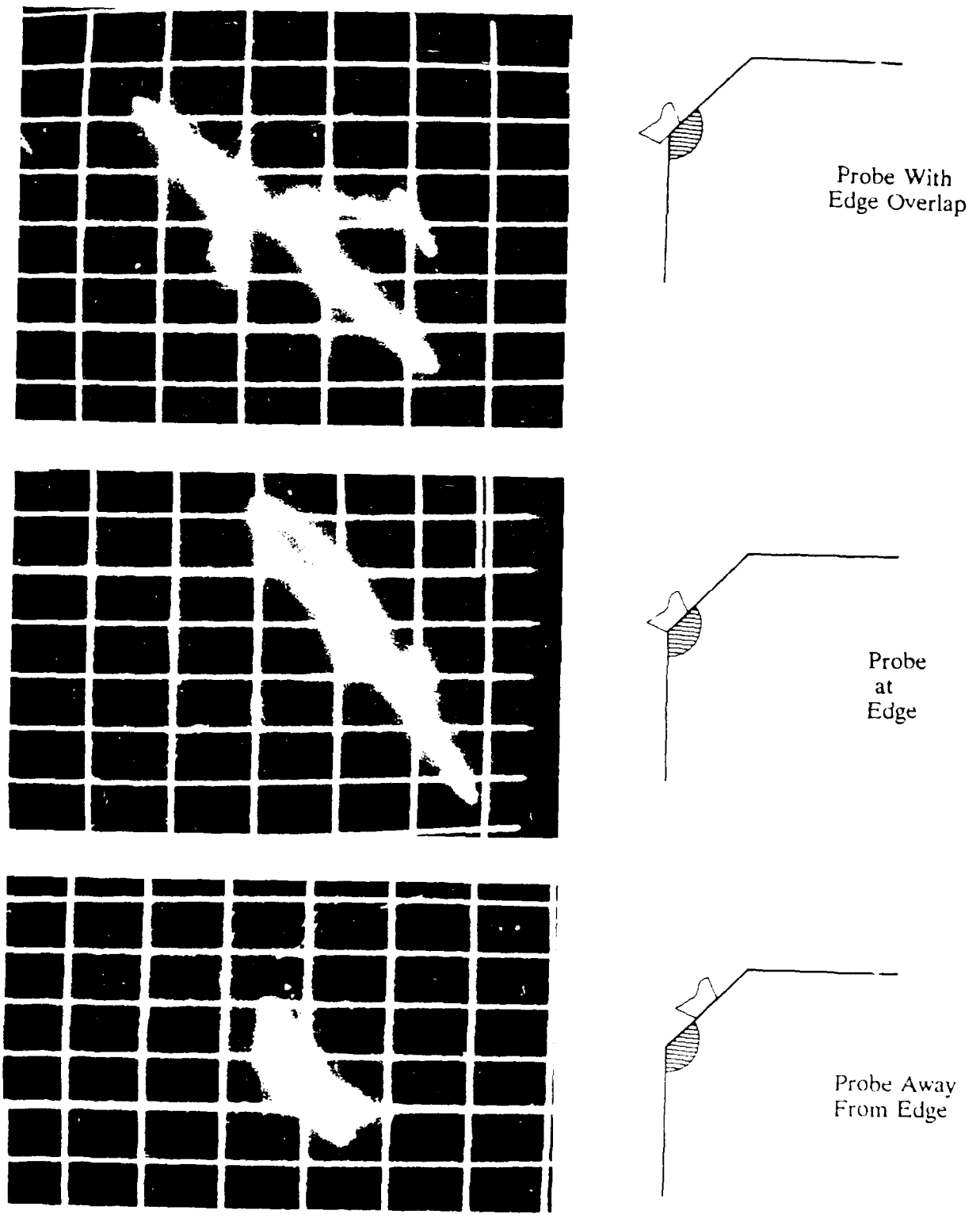

Figure 9. Geometry and flaw position effects

9.4 It is acceptable to vary the gain and indexing nut (position of the probe on the bevel) to analyze signals from flaws that may be low in amplitude such as flaws at the inner radius. Use the gain table and the setup procedure described in step 7.3.

9.5 Record these inspection parameter changes and data on the video tape immediately following the inspection and on Form NDT-10.

9.6 Record flaws on the resolution sheet, and note the approximate radial position and scan numbers of the flaw indication. Notes may also be added concerning approximate phase angle and magnitude.

9.7 The video tape may be used for post-inspection analysis on the monitor.

9.8 Fatigue cracks generally have smaller width lobes in the figure-eight flaw pattern (see Figure 10) when compared to the EDM notches (see Figure 7). Final judgment as to whether a pattern is a crack is up to the inspector.

10. DATA SHEETS

10.1 Calibration and inspection sheet, form No. NDT-9 (see Figure 11).

10.2 Resolution sheet, form No. NDT-10 (see Figure 12).

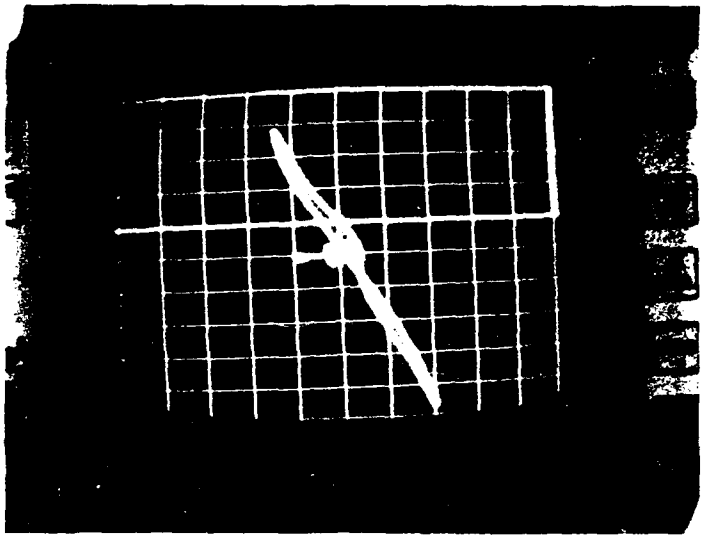

Figure-eight flaw pattern generated by an induced fatigue crack approximately 0.06 inch in depth

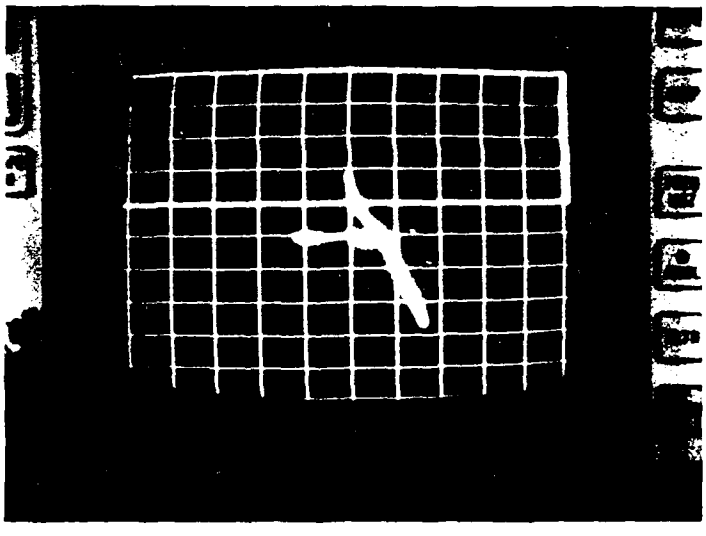

Figure-eight flaw pattern generated by an induced fatigue crack approximately 0.045 inch in depth

Figure 10. Fatigue crack signals

EDDY CURRENT INSTRUMENT CALIBRATION AND INSPECTION RECORD

Job #	Site	Date	Sheet No.
Examiner	Level	Procedure Rev.	Component Identification
Examiner	Level	Cal. Std. No.	Probe
Company		VIDEO TAPE RECORDER	
EDDY CURRENT PACKAGE		Model / S/N / Tape Speed	
NDT-19 S/N	Adt. Cable S/N	CALIBRATION VERIFICATION	

		Time	Tape Ct.	Wing No.	Aircraft No.	Comments	Initials
Frequency		Start					
Phase		Finish					
Filter		Start					
Vert. Gain		Finish					
Horz. Gain		Start					
REMARKS:		Finish					
		Start					
		Finish					
		Start					
		Finish					
		Start					
		Finish					

Reviewed by	Level	Date

Form NDT-9 Rev 0/Jan 89

Figure 11. Instrument calibration and inspection record sheet (Form NDT-9)

RESOLUTION DATA SHEET

Aircraft No. ____ Wing No. ____Left or Right _____ Date: _____

By: _____

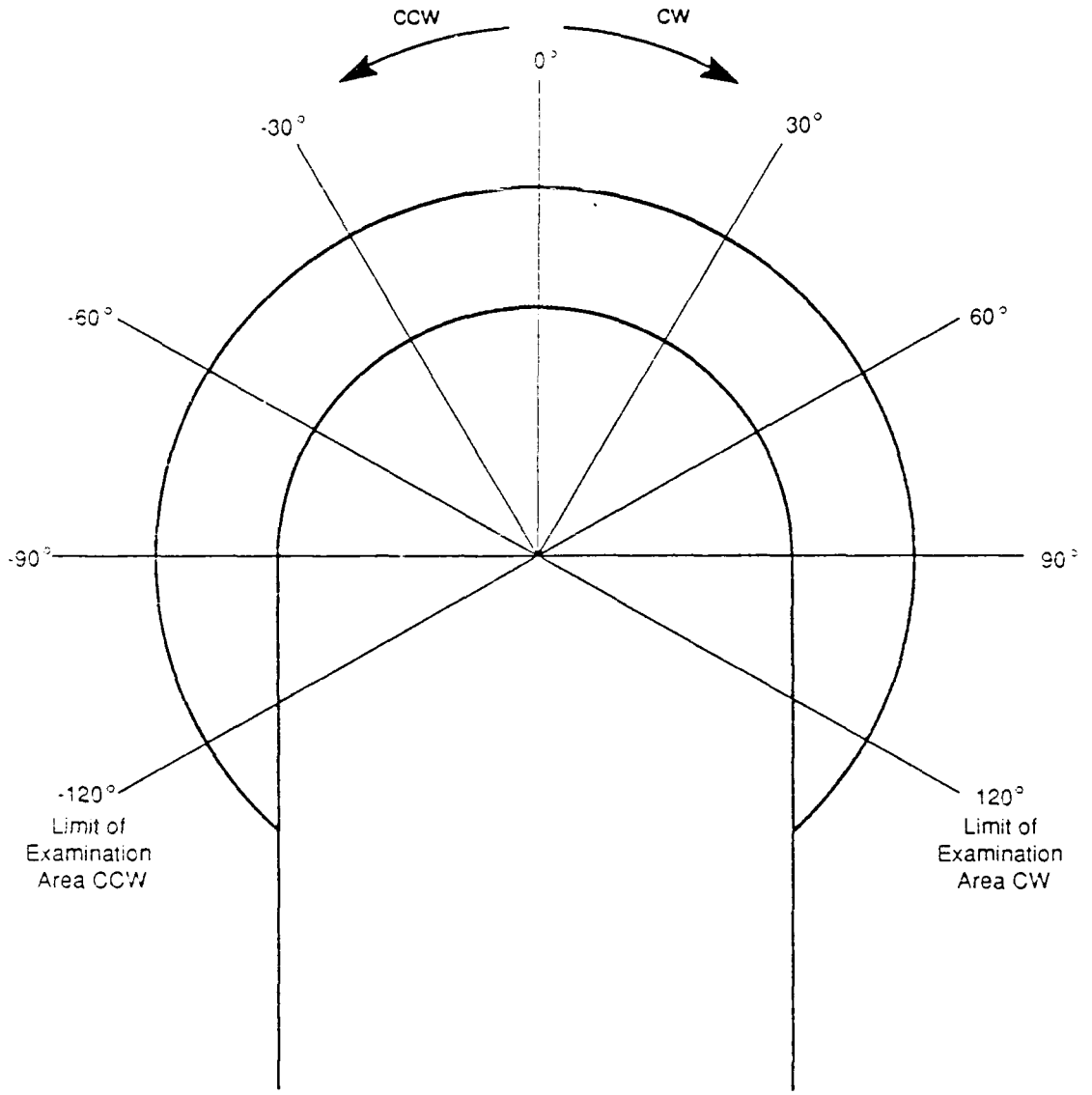

Comments:

Form NDT-10
Rev 0 12.88

Figure 12. Resolution sheet (Form NDT-10)